nature plants

Article

https://doi.org/10.1038/s41477-023-01391-3

Gibberellin and abscisic acid transporters facilitate endodermal suberin formation in *Arabidopsis*

Received: 18 May 2022

Accepted: 9 March 2023

Published online: 06 April 2023

Check for updates

Jenia Binenbaum[1], Nikolai Wulff[2], Lucie Camut[3], Kristian Kiradjiev[4,5], Moran Anfang[1], Iris Tal[1], Himabindu Vasuki[1,6], Yuqin Zhang[1], Lali Sakvarelidze-Achard[3], Jean-Michel Davière[3], Dagmar Ripper[7], Esther Carrera[8], Ekaterina Manasherova[9], Shir Ben Yaakov[1], Shani Lazary[1], Chengyao Hua[2], Vlastimil Novak[10], Christoph Crocoll[2], Roy Weinstain[1], Hagai Cohen[9], Laura Ragni[7], Asaph Aharoni[6], Leah R. Band[4,5] ✉, Patrick Achard[3] ✉, Hussam Hassan Nour-Eldin[2] ✉ & Eilon Shani[1] ✉

The plant hormone gibberellin (GA) regulates multiple developmental processes. It accumulates in the root elongating endodermis, but how it moves into this cell file and the significance of this accumulation are unclear. Here we identify three NITRATE TRANSPORTER1/PEPTIDE TRANSPORTER (NPF) transporters required for GA and abscisic acid (ABA) translocation. We demonstrate that NPF2.14 is a subcellular GA/ABA transporter, presumably the first to be identified in plants, facilitating GA and ABA accumulation in the root endodermis to regulate suberization. Further, NPF2.12 and NPF2.13, closely related proteins, are plasma membrane-localized GA and ABA importers that facilitate shoot-to-root GA_{12} translocation, regulating endodermal hormone accumulation. This work reveals that GA is required for root suberization and that GA and ABA can act non-antagonistically. We demonstrate how the clade of transporters mediates hormone flow with cell-file-specific vacuolar storage at the phloem unloading zone, and slow release of hormone to induce suberin formation in the maturation zone.

The phytohormone gibberellin (GA) is essential for many developmental processes in plants including seed germination, organ elongation and expansion through cell growth and division, trichome development, the transition from vegetative to reproductive growth, and flower, seed and fruit development[1]. GAs are produced mainly in the vasculature and move long distances in both acro- and basipetal directions[2–5]. The first reports of GA mobility through the phloem sap appeared over 50 years ago[6–8]. Grafting methods showed that biosynthesis of GA in the shoot

[1]School of Plant Sciences and Food Security, Tel Aviv University, Tel Aviv, Israel. [2]DynaMo Center of Excellence, Department of Plant and Environmental Sciences, University of Copenhagen, Frederiksberg, Denmark. [3]Institut de Biologie Moléculaire des Plantes, CNRS, Université de Strasbourg, Strasbourg, France. [4]Centre for Mathematical Medicine and Biology, School of Mathematical Sciences, University of Nottingham, Nottingham, UK. [5]Division of Plant and Crop Sciences, School of Biosciences, University of Nottingham, Sutton Bonington Campus, Loughborough, UK. [6]Department of Plant and Environmental Sciences, Weizmann Institute of Science, Rehovot, Israel. [7]ZMBP-Center for Plant Molecular Biology, University of Tübingen, Tübingen, Germany. [8]Instituto de Biología Molecular y Celular de Plantas, CSIC-UPV, Valencia, Spain. [9]Department of Vegetable and Field Crops, Institute of Plant Sciences, Agricultural Research Organization (ARO), Volcani Center, Rishon Lezion, Israel. [10]Plant Nutrients and Food Quality Research Group, Department of Plant and Environmental Sciences, University of Copenhagen, Frederiksberg, Denmark. ✉e-mail: leah.band@nottingham.ac.uk; patrick.achard@ibmp-cnrs.unistra.fr; huha@plen.ku.dk; eilonsh@tauex.tau.ac.il

can rescue GA biosynthesis mutations in the hypocotyl and root and vice versa[6–8]. In tobacco plants, defoliation results in internode elongation, cambial activity and fibre differentiation phenotypes that are similar to treatment with paclobutrazol, a GA biosynthesis inhibitor[5]. Another example of an organ dependent on an external source of GA are the petals, which require the anthers as their GA source[9,10]. The biosynthesis of active GA is a complex multistep process with diverse intermediates[11]. A series of grafting experiments using *Arabidopsis thaliana* mutant plants compromised at different stages of GA biosynthesis identified GA_{12} as the major GA form transported over a long distance through the vasculature[12]. GA_{12} moves through the xylem in a root-to-shoot manner and in the phloem in a shoot-to-root direction to regulate plant growth[12]. The translocation of GA_{12} from the root to the shoot is enhanced under ambient temperatures to induce shoot growth[13]. The transporters that regulate GA long-distance transport in the plant remain unknown.

In recent years, a number of *Arabidopsis* GA plasma membrane importers have been identified: two from the SWEET family and several others from the NITRATE TRANSPORTER1/PEPTIDE TRANSPORTER (NPF) family[14–17]. There are 53 NPFs in *Arabidopsis*, divided into 8 subfamilies. These proteins can transport a large variety of substrates such as nitrate, glucosinolates, abscisic acid (ABA), auxin and GAs[14,18,19]. Similar to auxin, GA is subjected to the ion-trap mechanism, limiting its ability to move out of cells. The existence of GA efflux transporters is therefore predicted to allow GA cell-to-cell movement[20]; however, no GA efflux transporters have been discovered[21].

ABA, which regulates growth and stress responses, has been long thought to act antagonistically to GA in processes such as seed germination, seed maturation and dormancy, and in responses to external cues[22–24]. Both GA and ABA induce developmental responses specifically from the endodermis[25–27]. GA accumulates at high levels in the endodermal cells of the root elongation zone[28]. The process is dependent on the activity of NPF3.1 (NPF3, *AT1G68570*), a member of the NPF family, which has been shown to act as a dual-specificity GA and ABA importer[16,29]. The endodermis, the innermost cortical layer that surrounds the central vasculature, goes through two phases of differentiation: the first step involves polar localized lignin deposition, which results in the formation of the casparian strips, and the second is the deposition of suberin as a lamella below the primary cell wall[30]. The casparian strips restrict apoplastic diffusion of water and nutrients into the vascular tissues, whereas suberin limits backflow of nutrients from the stele[31,32]. The physiological relevance of GA accumulation in the endodermis remains unknown.

With this study, we identified a sub-clade of NPF transporters that orchestrates GA_{12} long-distance shoot-to-root translocation and promote bioactive ABA and GA movement from the vasculature to the endodermis, which is required for endodermal suberization, a phenotype rescued by applying either ABA or GA. The importance of the transporter distributions was evaluated via a multicellular mathematical model that suggests an intriguing slow-release mechanism whereby GA and ABA delivered to the root in the phloem unloading zone are loaded into pericycle vacuoles and then slowly released to induce suberin formation in the maturation zone. Together, our findings reveal the mechanism that facilitates long-distance shoot-to-root movement of GA_{12} and explain how bioactive GA_4 and ABA are transported from the vasculature to the endodermis to mediate endodermal suberization.

Results

NPF2.14 is a tonoplast-localized GA and ABA transporter

To identify the missing GA exporters in plants, we tested whether NPF proteins are capable of GA_4 export in *X. laevis* oocyte-based transport assays. All other GA transporters identified so far import GA[14,33]. The transport assays investigate whether NPFs lead to efflux of GA that is loaded into oocytes by three different approaches, namely diffusion, injection and import by a GA importer. Oocytes expressing various *NPFs* or control oocytes injected with water were exposed to an array of membrane-permeable GAs (GA_4, GA_7, GA_9 and GA_{12})[34]. The screen identified NPF2.14 (*AT1G69860*) as a potential GA exporter. At the end of the assay, NPF2.14-expressing oocytes contained significantly reduced GA levels compared with control oocytes (Fig. 1a). This suggests that NPF2.14 facilitates the export activity of GAs out of oocytes. This was confirmed in an injection-based assay in which GA_3, a non-membrane-permeable form of GA, was injected directly into the oocyte. At the end of the assay, there was a lower GA_3 content in NPF2.14-expressing oocytes compared with control oocytes (Fig. 1b). Co-expression of both *NPF2.14* and *NPF4.1* (*AT3G25260*), which encodes a known GA importer, led to a reduced accumulation of non-membrane-permeable GA_3 compared with oocytes expressing only *NPF4.1* (Fig. 1c), further supporting the idea that NPF2.14 exports GA out of *X. laevis* oocytes.

It was previously shown that NPF3.1 transports both GA and ABA in *X. laevis* oocytes[16]. To test whether NPF2.14 also has dual-substrate specificity, control and NPF2.14-expressing oocytes were exposed to ABA. NPF2.14-expressing oocytes accumulated less ABA than did control oocytes (Fig. 1d), indicating that NPF2.14 has dual-substrate transport

Fig. 1 | NPF2.14 is a vacuolar GA and ABA transporter. a, GA accumulation in NPF2.14-expressing and control oocytes exposed to the indicated GAs at 50 µM concentration for 60 min at room temperature at pH 5 for GA_4 ($P = 0.0031$) and GA_7 ($P = 0.001$) and at pH 6 for GA_9 ($P < 0.0001$) and GA_{12} ($P = 0.0004$). Mean + s.e. ($n = 5$ for GA_4, GA_7 and GA_9 and $n = 6$ for GA_{12}). Two-tailed *t*-test (***$P < 0.005$). **b**, GA accumulation at 20 h after direct injection of 23 nl of 8.2 mM membrane-impermeable GA_3 at pH 7.4 at 16 °C (*t*1) and after 60 min at room temperature at pH 5 (*t*2). Mean + s.e. ($n = 6$ single oocytes). Two-way analysis of variance (ANOVA) with Holm Sidak post hoc test to adjust for multiple comparisons ($P \leq 0.05$). Different letters indicate statistically significant groups. **c**, GA accumulation in control oocytes or oocytes that express NPF2.14, NPF4.1 or both proteins exposed to 50 µM GA_3 at pH 5 for 60 min at room temperature and analysed by LC–MS/MS (liquid chromatography coupled to tandem mass spectrometry). Mean + s.e. ($n = 7$ single oocytes). Holm Sidak one-way ANOVA ($P = 0.05$). **d**, ABA accumulation in oocytes exposed to 50 µM ABA at pH 5 for 60 min at room temperature ($n = 5$ single oocytes). Two-tailed *t*-test ($P = 0.05$). **e**, Nitrate accumulation in oocytes exposed to 5 mM nitrate at pH 5 at room temperature for 60 min. Mean + s.e. (3 replicates of 5 oocytes analysed by analytical anion chromatography, $n = 3$). Holm Sidak one-way ANOVA ($P = 0.05$). **f**, Internal oocyte pH measured using three-electrode voltage clamp electrophysiology of control oocytes and NPF2.14- and NPF7.3-expressing oocytes. Oocytes were perfused at pH 7.4 for 5 min followed by perfusion at pH 5 for 5 min. Mean + s.e. ($n = 4$ oocytes for Mock and NPF2.14, 6 for NPF7.3). Holm Sidak one-way ANOVA ($P = 0.05$). **g**, Left: membrane potentials of control oocytes ($n = 12$) and NPF2.14-expressing oocytes ($n = 19$) measured at pH 5 using two-electrode voltage clamp electrophysiology. Right: oocytes with measured membrane potential were exposed to 50 µM GA_4 at pH 5 ($n = 7$ single oocytes) for 60 min at room temperature and analysed by LC–MS/MS. Mean + s.e. Two-tailed *t*-tests (***$P < 0.001$). **h**, GA accumulation in control oocytes or oocytes that express NPF2.14 with wild-type or mutant ExxE[K/R] motifs exposed to 50 µM GA_4 at pH 5 for 60 min at room temperature and analysed by LC–MS/MS ($n = 7$ oocytes). Mean + s.e. Holm Sidak one-way ANOVA ($P = 0.05$). Different letters indicate for statistically significant groups. **i**, Left: representative images of 6-day-old *npf2.14* mutant and *npf2.14* complementation lines. Roots were treated with 5 µM GA_3-Fl (yellow); PI, pink. Right: GA_3-Fl fluorescence intensity in the endodermis, mean ± s.e. (5 endodermal cells sampled from each root, $n = 50$ for Col-0, 40 for *npf2.14* and 30 for *pNPF2.14:NPF2.14-GFP/npf2.14*). **j**, GA_4 (left) ($P = 0.0002$) and ABA content (right) ($P = 0.0024$) in 10-day-old roots of control and *npf2*.14 mutant plants measured using LC–MS. Each replicate is 200 mg of pooled *Arabidopsis* roots. Mean + s.e. ($n = 5$). Two-tailed Student's *t*-test (**$P < 0.01$). **k**, Representative confocal image of 6-day-old root epidermis of *35S:NPF2.14-YFP* cells stained with PI (red) and tonoplast marker Vac-CFP (cyan)[1]. The experiment was repeated 3 times with similar results.

https://doi.org/10.1038/s41477-023-01391-3

activity. Several NPF transporters, including NPF6.3 (*AT1G12110*), also transport nitrate[18], but NPF2.14 displayed no nitrate transport activity in oocyte assays (Fig. 1e).

NPF7.3 has recently been shown to lower the cytoplasmic pH in *X. laevis* oocytes, which can indirectly influence the accumulation equilibrium of weak acids such as GA and ABA[34]. To assess whether

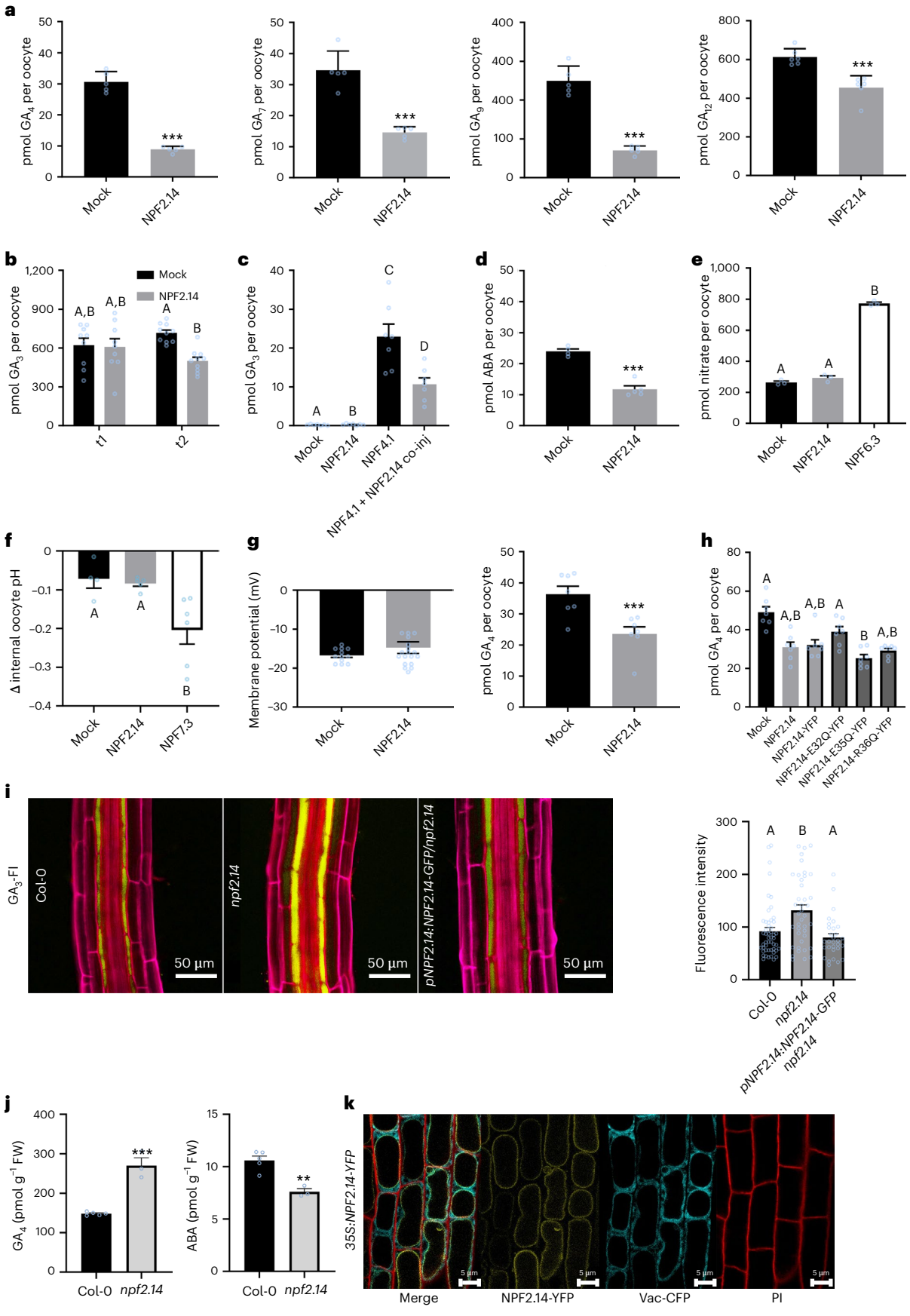

NPF2.14 has a similar activity, we measured the intracellular oocyte pH using a proton-selective three-electrode voltage clamp setup. We showed that, unlike NPF7.3, NPF2.14 expression in the oocyte does not alter the internal oocyte pH (Fig. 1f). Another factor that can theoretically lead to a false-positive GA export result is alteration of membrane potential. Therefore, we measured the membrane potential of control and NPF2.14-expressing oocytes using a two-electrode voltage clamp setup. The membrane potential of control and NPF2.14-expressing oocytes were both approximately −15 mV (Fig. 1g). When oocytes were subjected to GA_4 for 60 min before membrane potential measurement, less GA was observed in NPF2.14-expressing oocytes than in control oocytes (Fig. 1g). Thus, NPF2.14 does not shift oocyte membrane potential.

Many NPF proteins, including NPF2.14, contain the ExxE[K/R] motif[35], which is involved in coupling substrate transport to the proton gradient across membranes[36]. Involvement of the ExxE[K/R] motif in NPF2.14-mediated effluxes would suggest antiporter function. To assess the involvement of the ExxE[K/R] motif, we generated C-terminal Yellow Fluorescent Protein (YFP) YFP-tagged NPF2.14 mutants substituted at each of the three charged residues with a polar but uncharged residue. The YFP-tag alone did not influence the apparent GA_4 transport by the wild-type NPF2.14 (Fig. 1h). When any of the charged residues of the ExxE[K/R] motif was replaced with the polar uncharged Gln residue, no significant difference in GA_4 transport was observed compared with wild-type NPF2.14 (Fig. 1h). Thus, the GA_4 transport mediated by NPF2.14 seems to be ExxE[K/R] motif independent.

To test whether the *X. laevis* oocyte GA transport data are physiologically relevant in planta, we isolated a homozygous T-DNA knockout line for *NPF2.14*. The single *npf2.14* mutant did not show notable shoot or root growth phenotypes (Supplementary Fig. 1a,b). Several NPF family members transport nitrate, including NPF6.3[37]. Thus, despite having shown that NPF2.14 does not transport nitrate in oocytes (Fig. 1d), we checked whether *npf2.14* mutants display an impaired growth on low-nitrate media. *npf2.14* T-DNA insertion mutants did not have a visible growth phenotype and did not differ from Col-0 plants under low-nitrate conditions (Supplementary Fig. 1c). To determine whether NPF2.14 is involved in GA distribution and accumulation in the root, we tested whether the distribution of a fluorescently tagged GA_3 compound (GA_3-Fl) was affected in the loss-of-function line. GA_3-Fl has been developed in our lab to serve as a stable bioactive reporter to study GA movement/accumulation in planta[28]. Accumulation of GA3-Fl in the endodermis was visible in the Col-0 plants, as previously shown[28]. The *npf2.14* mutants displayed a significantly stronger signal compared with the Col-0 control (Fig. 1i). This enhanced accumulation was restored to normal levels when expressing *NPF2.14* driven by its native promoter (*pNPF2.14:NPF2.14-GFP*) on the background of the *npf2.14* T-DNA line (Fig. 1i), indicating that loss of NPF2.14 affects GA3-Fl distribution in the plant. In agreement with this result, *npf2.14* mutants accumulated significantly higher levels of GA_4 in their roots (Fig. 1j).

To test whether NPF2.14 has a dual-specificity function and can also import ABA, we tested the distribution of the fluorescently tagged ABA (ABA-Fl) in the roots. ABA-Fl has very low bioactivity, but can be utilized to estimate ABA movement in the plant[33]. In addition, we quantified endogenous levels of ABA in the roots. We found that similar to GA-Fl, *npf2.14* mutants accumulated significantly high levels of ABA-Fl in their root endodermis cells (Supplementary Fig. 2), but showed low levels of native ABA (extracted from the entire root) (Fig. 1j).

To study the subcellular localization of NPF2.14, we generated and imaged *35S:NPF2.14-YFP* lines. Interestingly, NPF2.14 localized to the tonoplast vacuole membrane (Fig. 1k). Therefore, although we had hypothesized that NPF2.14 was a GA exporter that transported GA from inside the cytosol to the apoplast, the protein is instead a tonoplast-localized transporter. To the best of our knowledge, this is presumably the first report of a subcellular GA/ABA transporter.

NPF2.14 regulates suberin formation in the root endodermis

To characterize NPF2.14 expression patterns in the plant, we generated NLS-YFP and GUS reporter lines driven by the *NPF2.14* promoter. Confocal imaging of the NLS-YFP lines indicated that NPF2.14 is expressed only in the pericycle of the root mature zone, mainly at the phloem poles and not in the meristematic zone (Fig. 2a and Supplementary Fig. 3a). In addition, GUS staining showed expression in the shoot vasculature in seedlings (Supplementary Fig. 3b). To test whether GA or ABA affects NPF2.14 expression patterns, we examined *pNPF2.14:GUS* lines after an exogenous treatment of GA_3 (5 µM) or ABA (1 µM). While GA did not affect *pNPF2.14:GUS* staining, we observed a stronger staining in the ABA treatment, yet expression remained in the vasculature (Supplementary Fig. 4). In the mature stages, the *NPF2.14*-driven reporter was expressed in the periderm (Supplementary Fig. 3c). The pericycle is a deep layer of post-embryonic meristematic cells encircling the vascular tissue[38]. In the root, it is required for lateral root emergence[39], xylem loading[40] and phloem unloading[41]. At later stages, it gives rise to the periderm, which serves as the outer protective layer when the surrounding tissue is sloughed off[38]. Both the endodermis and the cork, which is the outermost cell layer of the periderm, are suberized tissues[42].

The expression of the reporter driven by the *NPF2.14* promoter in a tissue that undergoes suberization, taken together with the ability of NPF2.14 to transport ABA, which has been previously shown to regulate suberin deposition[43], led us to hypothesize that this transporter might facilitate root suberization.

To test this, we analysed suberization in *npf2.14* T-DNA mutants using Nile red and Fluorol yellow, which are suberin dyes[44,45]. Suberization commences in the endodermis of the upper part of the maturation zone of the root and, as the plant matures more cells undergo suberization[46]. Quantification of Nile red and Fluorol yellow fluorescence intensity in the uppermost part of 5-day-old roots revealed that the mutant *npf2.14* plants had significantly lower levels of endodermal suberin than Col-0 plants (Fig. 2b and Supplementary Fig. 5). In addition, Col-0 plant roots showed a typical pattern of suberin formation with a non-suberized zone, followed by a suberizing zone where only patches of endodermal cells are suberized (patchy suberization) and a continuous suberized zone. We found significant reduction in the continuously suberized zone for *npf2.14* T-DNA and an additional CRISPR *npf2.14* allele we generated (Fig. 2c). Suberin levels remained lower compared with Col-0 at later stages of development, including 10-day-old roots and 3-week-old hypocotyls (Supplementary Fig. 6), showing that the reduction of suberin deposition in the endodermis is stable over time and that also cork suberin is affected.

Suberin is a complex polyester based on glycerol and long-chain α,ω-diacids and ω-hydroxyacids[47], and is primarily found in structures such as the periderm, endodermis and seed coat[30]. To examine changes in root suberin composition between *npf2.14* and Col-0, we analysed their suberin monomer profiles via gas chromatography–mass spectrometry (GC–MS). We found significant reductions in ferulic acid, the predominant aromatic component of suberin, as well as in C22 fatty acid and C18:1(9) ω-hydroxyacid—two of the most abundant suberin building blocks in the *Arabidopsis* root endodermis (Fig. 2d). In addition, C18 ester was lower in *npf2.14* roots. These reductions accompanied by lower levels of other monomers resulted in 35% less total suberin contents in the mutant roots (Fig. 2d). Overall, these findings provide several lines of evidence that alteration of NPF2.14 has a substantial effect on suberin deposition in the root endodermis.

Similar to the *npf2.14* mutant, *npf3.1* mutant plants, which have been shown to have impaired GA and ABA delivery to the endodermis[16], displayed reduced suberization levels compared with Col-0 plants (Supplementary Fig. 7). GA or ABA treatments completely rescued the *npf2.14* mutant suberization levels (Fig. 2b).

Endodermal suberization is regulated by ABA perception, both under normal and stress conditions[43,48]. ABA treatment was previously reported to induce endodermal suberization[49]. In agreement with

https://doi.org/10.1038/s41477-023-01391-3

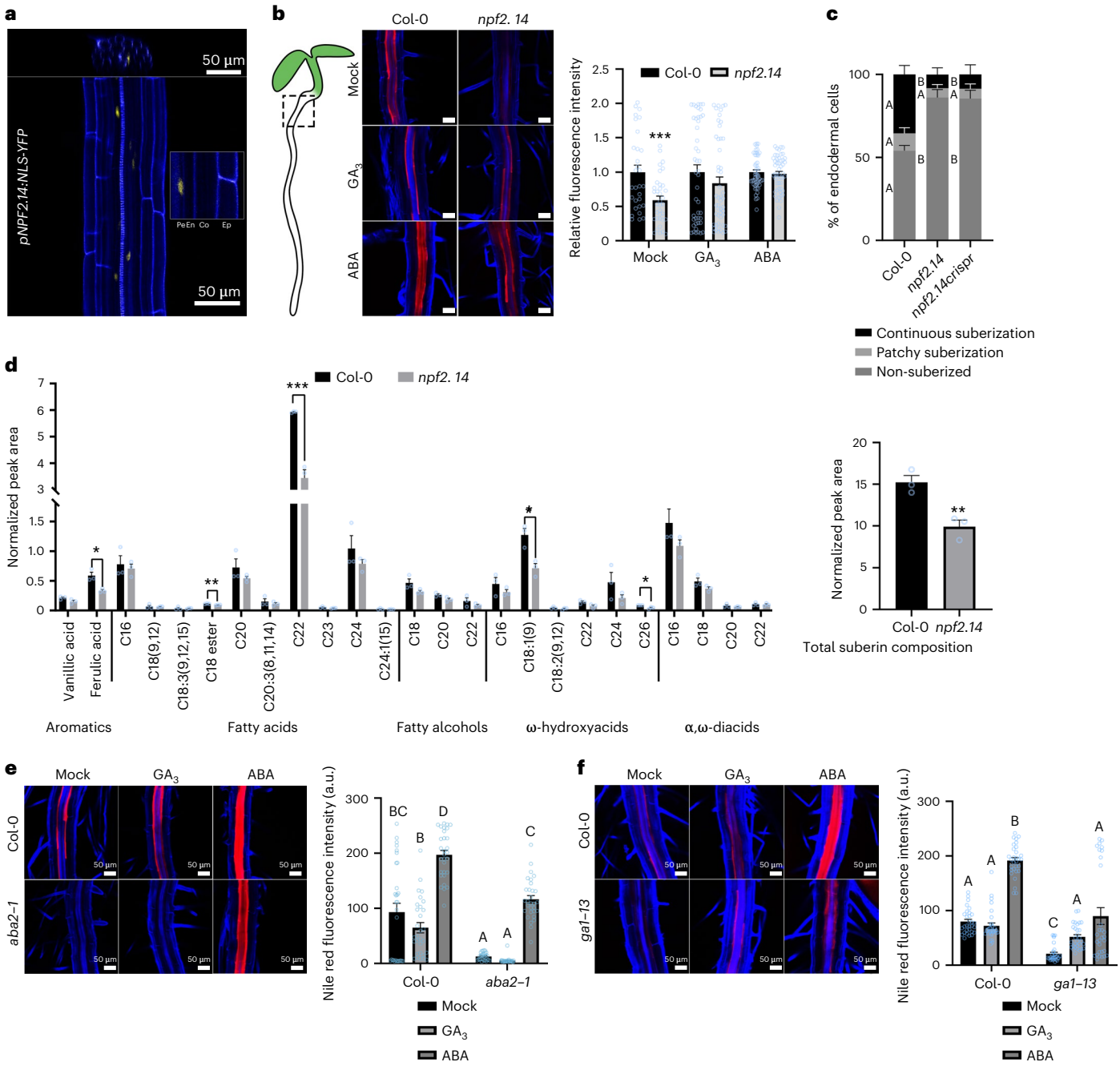

Fig. 2 | *NPF2.14* expression in differentiated pericycle is required for endodermal root suberization. a, Confocal image of 6-day-old *pNPF2.14:NLS-YFP* roots stained with PI (blue) and imaged for YFP (yellow). Inset is magnification of cells with *pNPF2.14:NLS-YFP* signal. Pe, pericycle; En, endodermis; Co, cortex; Ep, epidermis. The experiment was repeated 3 times with similar results. **b**, Left: images of 5-day-old Col-0 and *npf2.14* mutant roots supplemented with mock solution, 5 µM GA_3 or 1 µM ABA and stained with Nile red (red) and calcofluor (blue). Right: quantification of Nile red fluorescence intensity, normalized to Col-0. Mean + s.e. Dashed box in illustration indicates imaged area. Fluorescence intensity quantified from 5 endodermal cells per root, minimum of 6 roots per treatment ($n = 30$ for Mock-treated Col-0, 35 for Mock-treated *npf2.14* and GA_3-treated Col-0; $n = 50$ for the rest). Two-way ANOVA followed by Sidaks's post hoc multiple comparisons test (***$P = 0.003$). **c**, Quantification of suberin pattern along the root using Nile red fluorescence intensity. Mean + s.e. ($n = 10$ individual plants). Two-way ANOVA with Dunnett's multiple comparisons post hoc test. Different letters indicate significant differences ($P < 0.0001$). **d**, Left: root suberin profile for 10-day-old plants, measured by GC–MS. The *y* axis represents relative peak areas following normalization to a C_{32}-alkane internal standard. Right: total suberin composition. Mean ± s.e. ($n = 3$). Two-tailed Student's *t*-test ($P = 0.0092$). Total suberin composition calculated by summing up all monomers. **e**, Left: images of 5-day-old Col-0 and *aba2-1* roots from plants grown on mock MS or MS with 1 µM ABA. Roots were stained with Nile red (red) and calcofluor (blue). Right: fluorescent intensity was quantified from 6 roots per treatment, 5 endodermal cells per root. Mean + s.e. ($n = 30$ individual cells). Two-way ANOVA with a Tukey's multiple comparisons post hoc test. Different letters mark significant differences ($P < 0.001$). **f**, Left: images of 5-day-old Col-0 and *ga1-13* mutant roots grown on mock MS or MS with 5 µM GA_3. Roots were stained with Nile red (red) and calcofluor (blue). Right: fluorescence intensity was quantified from 6 roots per treatment, 5 endodermal cells per root. Mean + s.e. ($n = 30$ individual cells). Two-way ANOVA with Tukey's multiple comparisons post hoc test. Different letters mark significant differences ($P < 0.05$).

https://doi.org/10.1038/s41477-023-01391-3

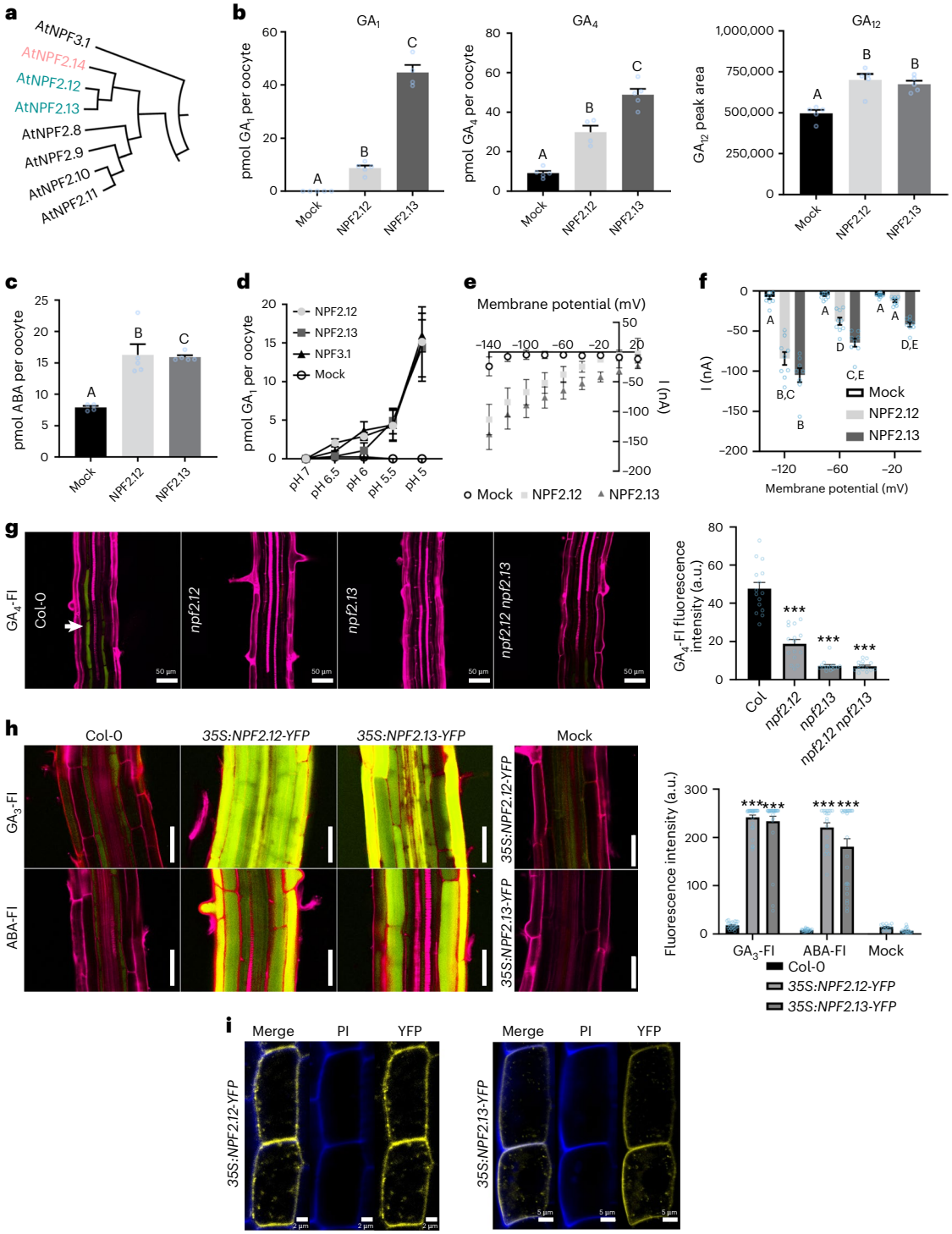

Fig. 3 | NPF2.12 and NPF2.13 are plasma membrane-localized GA and ABA importers that facilitate endodermal hormone accumulation. **a**, Phylogenetic clade of *NPF2.12, NPF2.13, NPF2.14* and their close paralogues. **b**,**c**, Hormone uptake in control and NPF2.12- and NPF2.13-expressing *Xenopus* oocytes. Mean + s.e. **b**, Oocytes were exposed to 50 µM GA_1 at pH 5 ($n = 5$ single oocytes), 50 µM GA_4 at pH 5.5 ($n = 5$) or 50 µM GA_{12} at pH 6 ($n = 5$). **c**, Oocytes were exposed to 50 µM ABA at pH 5 ($n = 5$). Hormone uptake analysed by LC–MS/MS. Holm Sidak one-way ANOVA ($P = 0.05$). **d**, Oocytes were exposed to 50 µM GA_1 at pH ranging from 5 to 7. Mean + s.e. ($n = 5$). **e**. IV (Current-Voltage) curve of GA-induced currents for mock (n = 10), NPF2.12 (n = 9) and NPF2.13 (n = 8) expressing oocytes exposed to 500 µM GA_3 at pH 5. Currents were measured using two-electrode voltage clamp electrophysiology over a range of membrane potentials from +20 to −140 mV. **f**. Representaiton of mean currents (from e) at three selected membrane potentials. Holm Sidak two-way ANOVA ($P = 0.01$). Different letters indicate statistically significant groups. **g**, Left: representative images of roots of 6-day-old Col-0 and single and double *npf2.12* and *npf2.13* knockout plants treated with 5 µM GA_4-Fl (yellow) overnight. Pink, PI; white arrow, GA_4-Fl signal. Right: quantification of GA_4-Fl fluorescence intensity in the endodermis, mean ± s.e. (5 endodermal cells per 3 biological repeats, $n = 15$). Two-way ANOVA with post hoc Dunnett's multiple comparisons test (***$P \leq 0.0001$). **h**, Left: representative images of roots of 6-day-old *35S:NPF2.12-YFP* and *35S:NPF2.13-YFP* plants treated with 5 µM GA_3-Fl or ABA-Fl for 2 h. Pink, PI; yellow, GA_3-Fl or ABA-Fl. Right: GA_3-Fl and ABA-Fl fluorescence intensity quantified in the epidermal cells, mean ± s.e. (5 epidermal cells sampled from at least 4 biological repeats, $n > 20$). *35S:NPF2.12-YFP* and *35S:NPF2.13-YFP* mock do not show fluorescence under these confocal gain settings. Two-way ANOVA followed by Dunnett's multiple comparisons test (***$P \leq 0.0001$). **i**, Confocal imaging of 6-day-old root meristem epidermal cells expressing *35S:NPF2.12-YFP* (left) and *35S:NPF2.13-YFP* (right). Blue, PI; yellow, YFP. The experiment was repeated 3 times with similar results.

this report, ABA significantly upregulated the Nile red fluorescence intensity in the root endodermis and rescued the reduced suberization observed in the *aba2-1* mutant (*AT1G52340*), which is deficient in ABA biosynthesis[49] (Fig. 2e). To the best of our knowledge, GA has not been previously associated with endodermal suberization. To establish whether GA regulates root suberization in *Arabidopsis* seedlings, we quantified suberization levels in GA-treated wild-type and *ga1-13* mutant plants using the Nile red dye. GA1 (*AT4G02780*) catalyses the first committed step in the GA biosynthetic pathway[50]. The GA biosynthesis mutant *ga1-13* displayed a significant reduction in suberization levels, which was restored by the exogenous application of GA_3 (Fig. 2f). Furthermore, while ABA treatment, but not GA treatment, can rescue and induce the reduced suberin levels of *aba2-1*, both ABA and GA can rescue the reduced suberin levels of *ga1-13* (Fig. 2e–f). Notably, GA treatment could only rescue the suberin back to wild-type levels and did not induce it to a higher level as ABA treatment did. GA and ABA have long been thought to have completely antagonistic functions[51]. Our results indicate that this antagonistic activity is more complex and that GA and ABA induce root suberization. Taken together, our data suggest that NPF2.14 is a pericycle-specific GA and ABA transporter localized to the tonoplast and involved in regulating GA and ABA accumulation in the endodermis to promote suberization.

NPF2.12 and NPF2.13 are plasma membrane-localized GA and ABA importers

NPF2.12 (*AT1G27080*) and its close paralogue *NPF2.13* (*AT1G69870*) form a phylogenetic sub-clade with *NPF2.14* (Fig. 3a and Supplementary Fig. 8). We hypothesized that due to this proximity on the phylogenetic tree, NPF2.12 and NPF2.13 might also contribute to GA and ABA accumulation in the endodermis. Both transporters were previously characterized as low-affinity nitrate transporters[52,53] and more recently, were shown to promote GA import activity in heterologous systems[14,34]. Neither have been characterized in plants as GA or ABA transporters. To test for direct GA transport activity of NPF2.12 and NPF2.13, we performed *X. laevis* oocyte-based transport assays. Oocytes expressing NPF2.12 or NPF2.13 accumulated significantly higher levels of GA_1, GA_3, GA_4, GA_7, GA_9, GA_{12}, GA_{19} and GA_{24} compared with control oocytes over the course of 60 min (Fig. 3b and Supplementary Fig. 9a). This suggests that NPF2.12 and NPF2.13 are promiscuous GA importers. Both NPF2.12- and NPF2.13-expressing oocytes also had higher levels of ABA accumulation than controls (Fig. 3c).

NPF2.12 and NPF2.13 both contain an ExxE[K/R] motif, which couples substrate transport to the proton gradient[36]. To test whether NPF2.12 and NPF2.13 substrate transport activity is coupled with external proton concentration, NPF2.12- and NPF2.13-expressing oocytes were exposed to membrane-impermeable GA_1 in solutions with pH ranging from 5 to 7 in 0.5 pH unit increments. In both NPF2.12- and NPF2.13-expressing oocytes, GA_1 accumulation increased as pH was lowered (Fig. 3d). These data indicate that GA transport by NPF2.12 and NPF2.13 is likely proton-coupled.

To investigate whether the transport of GA by NPF2.12 and NPF2.13 is electrogenic, we used two-electrode voltage clamp electrophysiology to evaluate oocytes that express the transporters. Subtracting the currents elicited by oocytes at different membrane potentials in the absence of GAs from the currents elicited by oocytes in the presence of 500 µM GA_3 revealed that GA_3 transport by both NPF2.12 and NPF2.13 is associated with negative currents relative to control oocytes (Fig. 3e). As the negative currents reflect a net positive influx of charges, this indicates at least a 2:1 proton:GA_3 stoichiometry if GA_3 is transported in its anionic form. However, it cannot be excluded that GA_3 may be transported in its neutral form. In non-clamped conditions, NPF2.13 displayed significantly higher uptake levels of GA_1 and GA_4 compared with NPF2.12. Similarly, currents elicited by NPF2.13-expressing oocytes were significantly higher compared with NPF2.12-expressing oocytes when oocytes were clamped at membrane potentials that mimic the membrane potential in the non-clamped uptake assays (Fig. 3e,f). However, at high negative membrane potential (−120 mV), GA_3-induced currents in NPF2.12-expressing oocytes were of the same magnitude as those in NPF2.13-expressing oocytes (Fig. 3e,f). This suggests that the transport activity of NPF2.12 is sensitive to alterations in the membrane potential (Fig. 2b). In agreement with previous publications[52,53], we detected nitrate import into oocytes that expressed NPF2.12 or NPF2.13, but this transport did not interfere with the GA transport capabilities as GA accumulation was not affected in GA/nitrate competition assays (Supplementary Fig. 9b). In continuation, we performed equimolar GA/ABA competition transport assays, which showed that ABA does not affect GA transport, whereas a slight but significant enhancement in ABA uptake was seen in NPF2.13-expressing oocytes when exposed simultaneously to GA_3. The data show that NPF2.12 and NPF2.13 are multispecific towards nitrate, ABA and GA, and suggests that GA might enhance NPF2.13 ABA transport activity (Supplementary Fig. 10). Multispecificity has emerged as an inherent property of the NPF family that is suggested to enable the tantalizing integration of environmental information to the availability of different nutrients[18]. Exhaustive structure–function studies are needed to decipher the molecular basis of the selectivity of these transporters.

To elucidate whether these transporters are part of the GA transport mechanisms in the plant, we treated T-DNA knockout lines, which did not display any visible phenotypes (Supplementary Fig. 11), with GA_4-Fl. *npf2.12* and *npf2.13* single mutant plants treated with GA_4-Fl displayed a significant reduction in accumulation in the endodermis compared with Col-0 plants (Fig. 3g), similar to reduced levels detected in *npf3.1* mutants. To verify that the reduction in GA-Fl accumulation was not due to an off-target mutation, we repeated the test with an additional *npf2.12* T-DNA insertion line (*npf2.12-2*) and obtained similar results (Supplementary Fig. 12a). In addition, homozygous *pNPF2.13:NPF2.13-YFP* plants completely rescued the root GA_3-Fl phenotype (Supplementary Fig. 12b).

We next generated plants ectopically expressing *NPF2.12* or *NPF2.13* fused to YFP (*p35S:NPF2.12-YFP* and *p35S:NPF2.13-YFP*, respectively) and treated them with GA_3-Fl. These lines showed a remarkably strong accumulation of GA_3-Fl in all root cells (Fig. 3h), supporting the hypothesis that NPF2.12 and NPF2.13 are GA transporters in planta. To test whether NPF2.12 and NPF2.13 have a dual-specificity function and can also import ABA (similar to NPF2.14), we treated plants with fluorescently tagged ABA (ABA-Fl)[33]. Overexpression of NPF2.12 or NPF2.13 resulted in extreme ABA-Fl accumulation compared with Col-0 plants (Fig. 3h), implying that both transporters import GA and ABA in planta.

Finally, to address the subcellular localization of NPF2.12 and NPF2.13, we imaged the root epidermis cells of *p35S:NPF2.12-YFP* or *p35S:NPF2.13-YFP* lines. Both NPF2.12 and NPF2.13 are localized to the plasma membrane (Fig. 3i). Together, the in planta and oocyte results indicate that NPF2.12 and NPF2.13 are dual-substrate, plasma membrane-localized GA and ABA importers.

NPF2.12 and NPF2.13 regulate root suberization

To further elucidate the biological function of NPF2.12 and NPF2.13, we generated NLS-YFP and GUS reporter lines to map NPF2.12 and NPF2.13 expression patterns. Confocal microscopy of plants expressing *NLS-YFP* driven by *NPF2.12* and *NPF2.13* native promoters revealed that in the root, NPF2.12 was expressed in the pericycle of the whole root and subsequently in the periderm of mature plants; NPF2.13, on the other hand, was expressed only in the shoot (Fig. 4a and Supplementary Fig. 13). Analysis of *pNPF2.12:GUS* and *pNPF2.13:GUS* lines showed that the two transporters are expressed in the shoot vasculature (Fig. 4b). GA or ABA treatment did not have a major effect on *NPF2.12* and *NPF2.13* expression level, as detected by qPCR and GUS reporter lines (Supplementary Fig. 14). The fact that the *NPF2.13* translational fusion construct (*pNPF2.13:NPF2.13-Venus*) introduced into the *npf2.13* mutant background rescued the root GA_3-Fl accumulation phenotype

https://doi.org/10.1038/s41477-023-01391-3

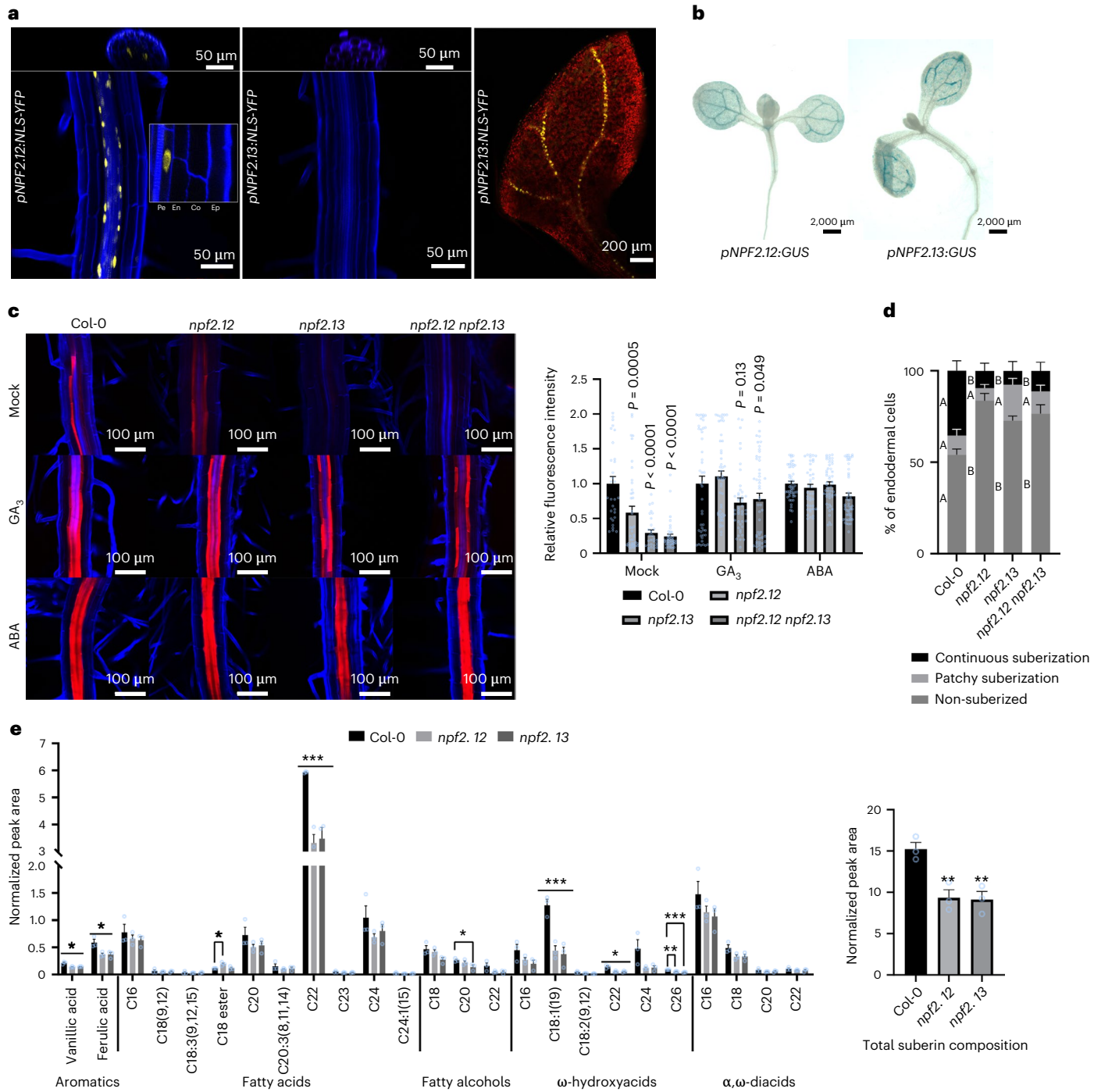

Fig. 4 | *NPF2.12* and *NPF2.13* regulate root endodermis suberization. **a**, Confocal imaging of 6-day-old *pNPF2.12:NLS-YFP* (left) and *pNPF2.13:NLS-YFP* (middle) seedlings. Inset is magnification of cells with *pNPF2.12:NLS-YFP* signal. Blue, calcofluor; yellow, YFP. Right: *pNPF2.13:NLS-YFP* cotyledon (red indicates chlorophyll). Experiments were repeated 3 times with similar results. **b**, GUS staining of 7-day-old seedlings expressing *pNPF2.12:GUS* and *pNPF2.13:GUS*. **c**, Left: Nile red-stained 5-day-old *npf* mutant roots mock-treated or treated with 5 µM GA_3 or 1 µM ABA. Right: fluorescent intensity relative to Col-0 quantified from a minimum of 6 roots per treatment, 5 endodermal cells per root ($n = 30$ for Mock-treated Col-0 and *npf2.13*, 40 for Mock and ABA-treated *npf2.12*, 45 for GA_3-treated Col-0 and *npf2.13*, and 50 for the rest). Two-way ANOVA followed by Dunnett's multiple comparisons test. **d**, Quantification of suberin pattern along the root using Nile red fluorescence intensity. Mean + s.e. ($n = 10$ individual roots). Two-way ANOVA with Tukey's multiple comparisons post hoc test. Different letters indicate significant differences between conditions ($P < 0.05$). **e**, Left: root suberin profile for 10-day-old plants, measured by GC–MS. The *y* axis represents relative peak areas following normalization to a C_{32}-alkane internal standard. Right: total suberin composition. Data in bars represent the means + s.e. of 3 biological replicates. Two-tailed Student's *t*-test (*$P \leq 0.015$, **$P \leq 0.01$ and ***$P \leq 0.001$ compared with Col-0). For total suberin composition, one-way ANOVA with Dunnett's multiple comparisons test ($P = 0.0072$ for *npf2.12*, $P = 0.006$ for *npf2.13*).

indicated that the promoter region we cloned is sufficient and that NPF2.13 expression is restricted to the shoot (Supplementary Fig. 12b). Similar to *npf2.14* mutants, *npf2.12* and *npf2.13* mutant plants displayed a reduction in suberization. Mutant roots stained with Nile red or Fluorol yellow showed a weaker fluorescence intensity than those in Col-0 plants (Fig. 4c and Supplementary Fig. 15). In agreement,

https://doi.org/10.1038/s41477-023-01391-3

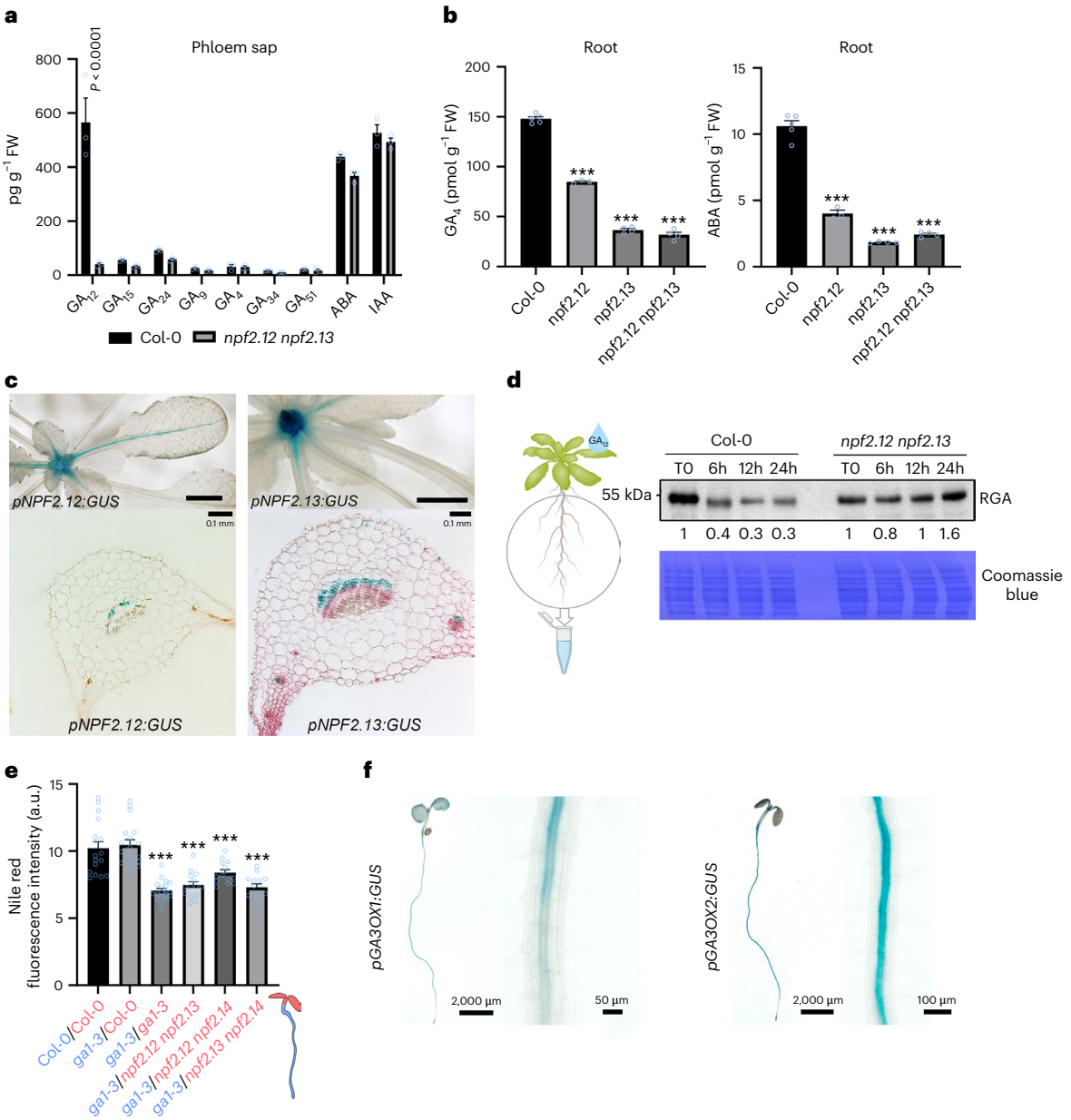

Fig. 5 | NPF2.12 and NPF2.13 facilitate long-distance shoot-to-root GA transport. a, Quantification of GA, ABA and IAA (indole-3-acetic acid) contents (in pg g^{-1} fresh weight) in phloem exudates collected from leaf petioles of 5-week-old Col-0 and *npf2.12 npf2.13* mutant plants. Mean + s.e. Exudate was collected from 75 leaves, pooled into 3 separate biological repetitions ($n = 3$). Statistical significance evaluated by Dunnett's multiple comparisons test, comparing to Col-0 as control ($P < 0.0001$). **b**, GA_4 (left) and ABA (right) quantification (in pmol g^{-1} fresh weight) in 10-day-old roots of Col-0 and *npf2.12 npf2.13* double-mutant plants. Mean + s.e. ($n = 5$). Two-way ANOVA followed by Dunnett's multiple comparisons test (***$P \leq 0.0001$). **c**, GUS-staining patterns in rosette leaves of 4-week-old *pNFP2.12:GUS* (left) and *pNPF2.13:GUS* (right) plants. Top: images of whole plants; scale bars, 0.25 cm. Bottom: images of cross-sections of GUS-stained leaf petioles; scale bars, 0.1 mm. **d**, Immunodetection of RGA protein accumulation in the root of 16-day-old Col-0 and *npf2.12 npf2.13* mutant plants. The plants were grown in vitro for 12 d and then moved to MS plates containing a low concentration of nitrogen (0.5 mM KNO_3) and paclobutratol (PAC, 1 µM). At 4 d after transfer, a drop of GA_{12} (5 µl at 1 µM) was added to one of the first two leaves formed. Proteins were extracted from the root at 4 time points following GA_{12} application. Similar results were obtained in two independent experiments. **e**, Quantification of Nile red fluorescence intensity (mean ± s.e.m.) of various combinations of grafted seedlings. Blue font, rootstock genotype; red, grafted scion. Fluorescence intensity was quantified from 5 roots per genotype/grafting, at least 3 endodermal cells per root, $n = 17$ for Col-0/Col-0, 18 for *ga1-3*/Col-0, 19 for *ga1-1/ga1-1* and 14 for the rest. Two-way ANOVA followed by Dunnett's multiple comparisons test (***$P < 0.001$). **f**, Images of 6-day-old plants that express GUS driven by the *GA3OX1-2* promoters. The experiment was repeated 3 times with similar results.

additional mutant alleles for *npf2.12* and *npf2.13* showed reduction in suberin level and patterning (Supplementary Fig. 16). Similar to *npf2.14* mutants, we detected a reduction in endodermal suberin levels of *npf2.12* and *npf2.13* 10-day-old roots and lower levels of cork suberin in 3-week-old *npf2.12 npf2.13* double-mutant hypocotyls stained with Fluorol yellow (Supplementary Fig. 17).

To test whether *NPF2.12* and *NPF.13* have partially redundant activities, we generated the *npf2.12 npf2.13* double mutant. The phenotype of the *npf2.12 npf2.13* double-mutant line was not enhanced compared to the single *npf2.12* and *npf2.13* mutants (Fig. 4c,d). We further generated additional double and triple mutant combinations with the *npf2.14* mutant via CRISPR genome editing (as *NPF2.14* is genetically linked

to *NPF2.13*) and tested their activity. We analysed suberin patterning for all genotypes and found that the phenotypes of the higher-order mutant knockouts were not enhanced compared to the single mutants (Supplementary Fig. 18). This result is in line with the fact that there is limited overlap among the three genes in terms of expression pattern or protein localization. Notably, GA_3 or ABA treatment completely rescued *npf2.12* low-suberin phenotype. The phenotypes of *npf2.13* and of the *npf2.12 npf2.13* double mutant were completely rescued by ABA and largely rescued by GA_3 (Fig. 4c). Quantification of suberin monomer content revealed that both *npf2.12* and *npf2.13* mutant roots accumulated ~40% less total suberin contents compared with the Col-0, attributed to lower levels of vanillic and ferulic acids, C22 fatty acid, C20 fatty alcohol, and C18:1(9), C22 and C26 ω-hydroxyacids (Fig. 4e).

NPF2.12 and NPF2.13 regulate shoot-to-root GA translocation

Our previous work showed that GA_{12}, although not bioactive, is the primary GA form transported over long distances through the vasculature in *Arabidopsis thaliana*[12]. GA_{12} can move through the xylem in a root-to-shoot manner and in the phloem in a shoot-to-root direction to regulate adaptive plant growth[12,13]. However, the mechanism regulating this process remains unknown[21]. NPF2.13 was expressed strictly in the shoot (Fig. 4a,b), yet the knockout led to a phenotype in the root endodermis (Fig. 4c). This led us to hypothesize that the transporters are involved in the long-distance shoot-to-root translocation of GA. To test whether NPF2.12 and NPF2.13 facilitate shoot-born GA loading into the phloem, we quantified GA content in phloem exudates collected from leaf petioles. The double *npf2.12 npf2.13* loss-of-function mutant showed a striking reduction in GA_{12} content in the collected phloem exudates (Fig. 5a). Other GA metabolites (GA_{15}, GA_{24}, GA_9, GA_4, GA_{34} and GA_{51}) were not significantly reduced (Fig. 5a). ABA levels showed a mild decrease, significant when compared to Col-0 using two-tailed *t*-tests, but not significant when using Dunnett's multiple comparisons test ($P \leq 0.05$). The results imply that NPF2.12 and NPF2.13 regulate GA and possibly ABA, loading into the shoot phloem. In agreement, quantification of active GA_4 (downstream of GA_{12} in the biosynthesis pathway) content in the root showed a significant reduction in the *npf2.12* and *npf2.13* single and double-mutant lines (Fig. 5b). ABA content was also significantly lower in mutant roots compared with Col-0 (Fig. 5b).

To further test this hypothesis, we examined the expression pattern of the two transporters using reporter lines. In mature rosette, *NPF2.12* and *NPF2.13* were expressed in the shoot apex and the main vascular vein (Fig. 5c). Cross-sections of *pNPF2.12:GUS* or *pNPF2.13:GUS* leaf petioles showed that both genes were expressed in the phloem companion cells (Fig. 5c). Next, we investigated whether these transporters are involved in long-distance GA movement from the shoot to the root. For this purpose, 16-day-old plants were grown on paclobutrazol, a GA biosynthesis inhibitor, for 4 d to deplete the plants of native GA and GA_{12} was applied to a single leaf. We then quantified the abundance of the DELLA growth repressing protein REPRESSOR OF GA1-3 (RGA, *AT2G01570*) in the root. DELLA proteins are central inhibitors of GA-regulated processes and GA relieves their inhibiting activity by activating their degradation[54]. Time-course experiments in Col-0 plants showed a significant reduction in RGA accumulation in the root after GA_{12} treatment, indicating GA_{12} movement from the shoot to the root (Fig. 5d). On the other hand, in the *npf2.12 npf2.13* double mutant, RGA abundance remained stable (Fig. 5d), signifying a reduced GA accumulation in the root.

To understand how NPF2.12/2.13/2.14-mediated long-distance GA transport influences root growth and suberin formation, we performed a series of micrografting between Col-0, different combinations of *npf* double mutants and GA-deficient *ga1-3* mutants and quantified both root elongation rate and Nile red fluorescence intensity. As expected, *ga1-3* self-grafts had shorter roots and displayed a significantly lower Nile red fluorescence intensity than the Col-0 self-grafts (Fig. 5e and Supplementary Fig. 19). Remarkably, *ga1-3* roots grafted to Col-0 shoots were indistinguishable from that of Col-0 self-grafts (Fig. 5e), supporting our hypothesis that GA can be transported from the shoot to the root to induce suberin formation. In comparison, *ga1-3* roots grafted to *npf2.12 npf2.13* shoots (*ga1-3/npf2.12 npf2.13*) were smaller and showed a reduction in suberization levels compared with *ga1-3*/Col-0, indicating a partial requirement of NPF2.12 and NPF2.13 in long-distance GA transport (Fig. 5e and Supplementary Fig. 19). Similarly, *npf2.12 npf2.14* and *npf2.13 npf2.14* double-mutant shoots grafted to *ga1-3* roots showed reduced suberin levels compared with *ga1-3*/Col-0. In addition, we found that GA_3-Fl application, specifically to the shoots of *npf2.12 npf2.14* double mutant or *npf2.14*, resulted in lower levels of GA_3-Fl in the roots of seedlings growing on paclobutrazol (Supplementary Fig. 20). These results further suggest that NPF2.12/13/14 contribute to long-distance shoot-to-root GA translocation.

We hypothesize that once GA_{12} is translocated to the roots, it can be converted to the bioactive GA_4 by the GA20ox and GA3ox enzymes, which are expressed in the root[55]. Profiling the expression pattern of the *GA3ox* promoters (*AT1G15550*, *AT1G80340*) catalysing the last step in bioactive GA_4 hormone synthesis showed that expression of these enzymes is restricted to the stele as previously reported[55] (Fig. 5f). Together, these results imply that NPF2.12 and NPF2.13 function in GA_{12} loading into the phloem for long-distance transport from the shoot to the root, with conversion to GA_4 taking place in the root stele.

Hormone storage in the phloem unloading zone facilitates suberization

To broaden our knowledge of GA and ABA distribution in the root and how it affects suberization, we created a mathematical model to simulate hormone distributions within the root cross-section, extending a modelling framework previously developed to study auxin transport[56]. Using a multicellular template segmented from a root-cross-sectional image (Supplementary Fig. 21), we incorporated into the model experimentally observed transporter distributions: NPF3.1 on endodermal cell membranes[16,29], NPF2.12 on pericycle cell membranes (Figs. 3i, 4a) and NPF2.14 on pericycle tonoplasts (Figs. 1k and 2a). The model simulated active hormone transport via NPF3.1, NPF2.12 and NPF2.14, passive hormone transport across both plasma membrane and tonoplast, hormone synthesis and degradation, and hormone diffusion within the apoplast with significantly reduced diffusion in the endodermal apoplast due to the presence of the Casparian strip. To parameterize the model, permeabilities associated with each passive and active transport component were estimated using the oocyte data, and transport rates were then specified on the basis of established pH and membrane potential values for plant cells[56–58] (Supplementary Table 5). An important factor is the source of the hormone. *ABA2* and *AAO3*, which encode enzymes necessary for ABA biosynthesis, were previously shown to be expressed in the vasculature[59]. Bioactive GA_4 is also synthesized at high levels in the *Arabidopsis* stele[55] (Fig. 5f). Considering these data, together with the phloem unloading zone[41] (the docking belt for the long-distance shoot-to-root transported hormones), led us to specify the stele as the source of active GA and ABA in the model.

We first used the model to test the hypothesis that the discovered clade of transporters is necessary and sufficient to explain the observed endodermal hormone accumulation. With all transporters present, the model predicts high levels of both cytoplasmic and vacuolar hormones in the endodermis (Fig. 6a for GA and Supplementary Fig. 22), consistent with the wild-type GA-Fl and ABA-Fl observations (Fig. 1i and Supplementary Fig. 2)[16] and where suberization later occurs. Mutations in *npf3.1* and *npf2.12* were predicted to have reduced endodermal hormone cytoplasmic concentrations (Fig. 6a and Supplementary Fig. 22), in agreement with the loss of endodermal GA-Fl in these mutants (Fig. 3g)[16] and explaining their reduced suberization (Fig. 4c, and Supplementary Figs. 7 and 15–18). We also considered NPF2.13 which is not expressed in the root (Fig. 4a) but contributes to the long-distance translocation of GA_{12}. Reducing long-distance translocation via the

https://doi.org/10.1038/s41477-023-01391-3

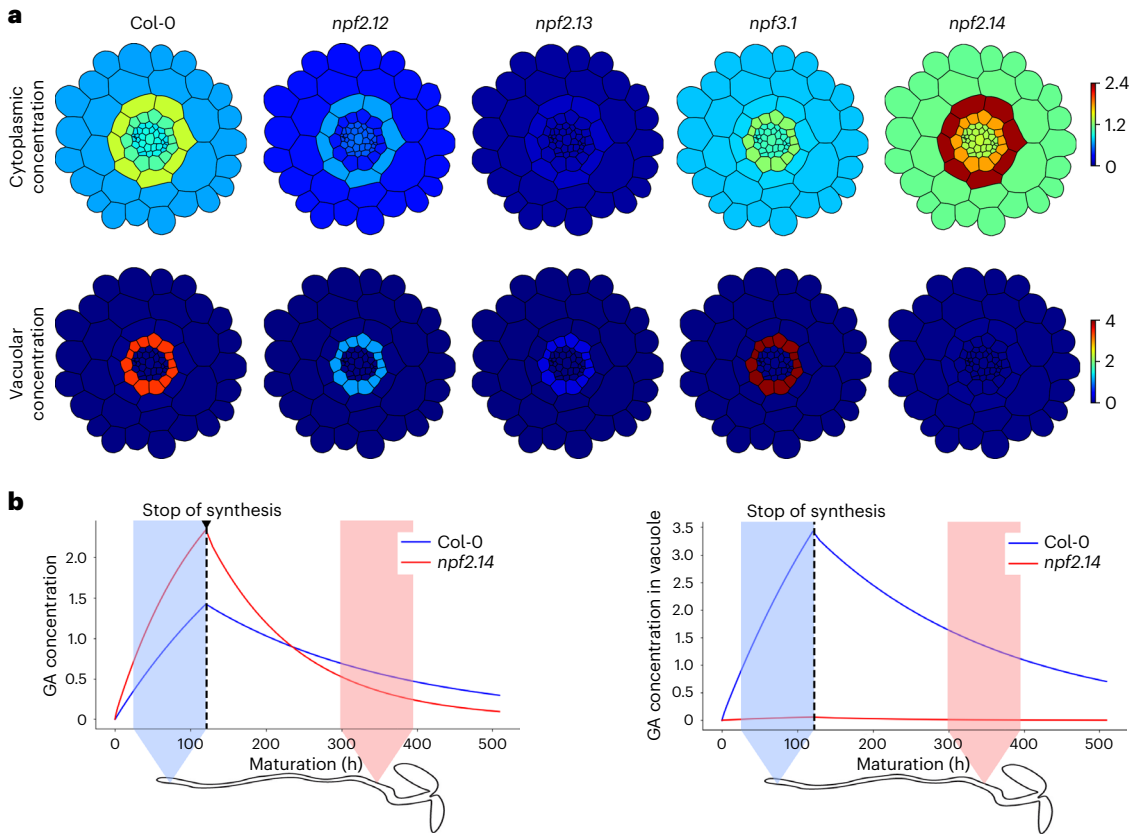

Fig. 6 | NPF transporters mediate pericycle-specific hormone uptake into the vacuoles at the phloem unloading zone to facilitate a hormone slow-release mechanism that allows suberization at the maturation zone. a, Spatial distributions of cytoplasmic and vacuolar GA concentration in the root cross-section, predicted by the multicellular mathematical model for the wild type and the *npf2.12*, *npf2.13*, *npf3.1* and *npf2.14* mutants. The time of the simulations is 5 d (120 h), corresponding to the age of the plants used in the experiments. Color bar indicates GA concentration (arbitrary units). **b**, Predicted dynamics of the endodermal cytoplasmic (left) and pericycle vacuolar (right) GA concentrations for the wild type and the *npf2.14* mutant. The model is initially simulated with a constant GA source in the stele (pale blue region), then synthesis is set to zero to simulate the GA redistribution after cells leave the phloem unloading zone. The model predicts that NPF2.14 leads to higher endodermal cytoplasmic concentrations, the endodermis being the region where suberin forms (pale red region).

npf2.13 mutation can be simulated by reducing the stele-specific synthesis rate, which leads to reduced predicted hormone concentrations throughout the root cross-section (Fig. 6a and Supplementary Fig. 22), again providing an explanation for the reduction in suberization (Fig. 4c and Supplementary Fig. 15–18). We concluded that NPF2.12, NPF2.13 and NPF3.1 all play distinct and necessary roles in creating the hormone accumulation within the endodermis that mediates suberization.

We then used the model to investigate the role of the tonoplast-localized NPF2.14. In contrast to the *npf2.12*, *npf2.13* and *npf3.1* mutations, simulations of the *npf2.14* mutation predicted endodermal cytoplasmic hormone concentrations that are higher than those in the wild type (Fig. 6a and Supplementary Fig. 22), in agreement with the GA-Fl accumulation at the elongation zone (Fig. 1i). Why *npf2.14* exhibits reduced suberization when endodermal accumulation is higher remains unclear. However, the model predictions revealed that the vacuolar concentrations in the *npf2.14* pericycle are much lower than in the wild type (Fig. 6a and Supplementary Fig. 23). These predictions led us to hypothesize that NPF2.14 regulates hormone levels both inside and outside of vacuoles that could provide a hormone source in the maturation zone, where the hormone is no longer supplied by the phloem yet is required for suberization. To test this hypothesis, we simulated the hormone dynamics after cells leave the phloem unloading zone, and found that the presence of NPF2.14 leads to higher predicted endodermal cytoplasmic concentrations as cells mature (Fig. 6b and Supplementary Fig. 24). This suggests that the tonoplast-pericycle-localized NPF2.14 ensures that endodermal hormone concentrations are at levels necessary to mediate suberization. Thus, on the basis of the model, we propose a pericycle-specific slow-release GA and ABA mechanism that explains how the two hormones are loaded into the pericycle vacuoles at the phloem unloading zone[41] and released from these vacuoles later on when the cells are mature (Fig. 6b). In this mechanism, GA and ABA unloaded from the phloem are transported into the pericycle and loaded into the vacuole to form a storage pool. When these cells reach the maturation zone, the GA and ABA that were stored in the pericycle vacuoles are transported by NPF3 into the endodermis to induce suberization.

In conclusion, the mathematical model revealed that the discovered clade of transporters is sufficient to explain the observed hormone distributions, with NPF3.1, NPF2.12 and NPF2.13 playing distinct and necessary roles for endodermal accumulation. Furthermore, the model revealed that the tonoplast-localized NPF2.14 facilitates vacuolar hormone accumulation within the pericycle, providing a source of hormones and enabling the cross-section to maintain high endodermal hormone levels after cells leave the phloem unloading zone[41]. Thus, the model predictions provide mechanistic explanations for the suberization phenotypes observed in the NPF mutants.

Discussion

In this work, we identified *NPF2.14*, a previously uncharacterized transporter, as a dual-specificity GA and ABA vacuolar transporter. To the

https://doi.org/10.1038/s41477-023-01391-3

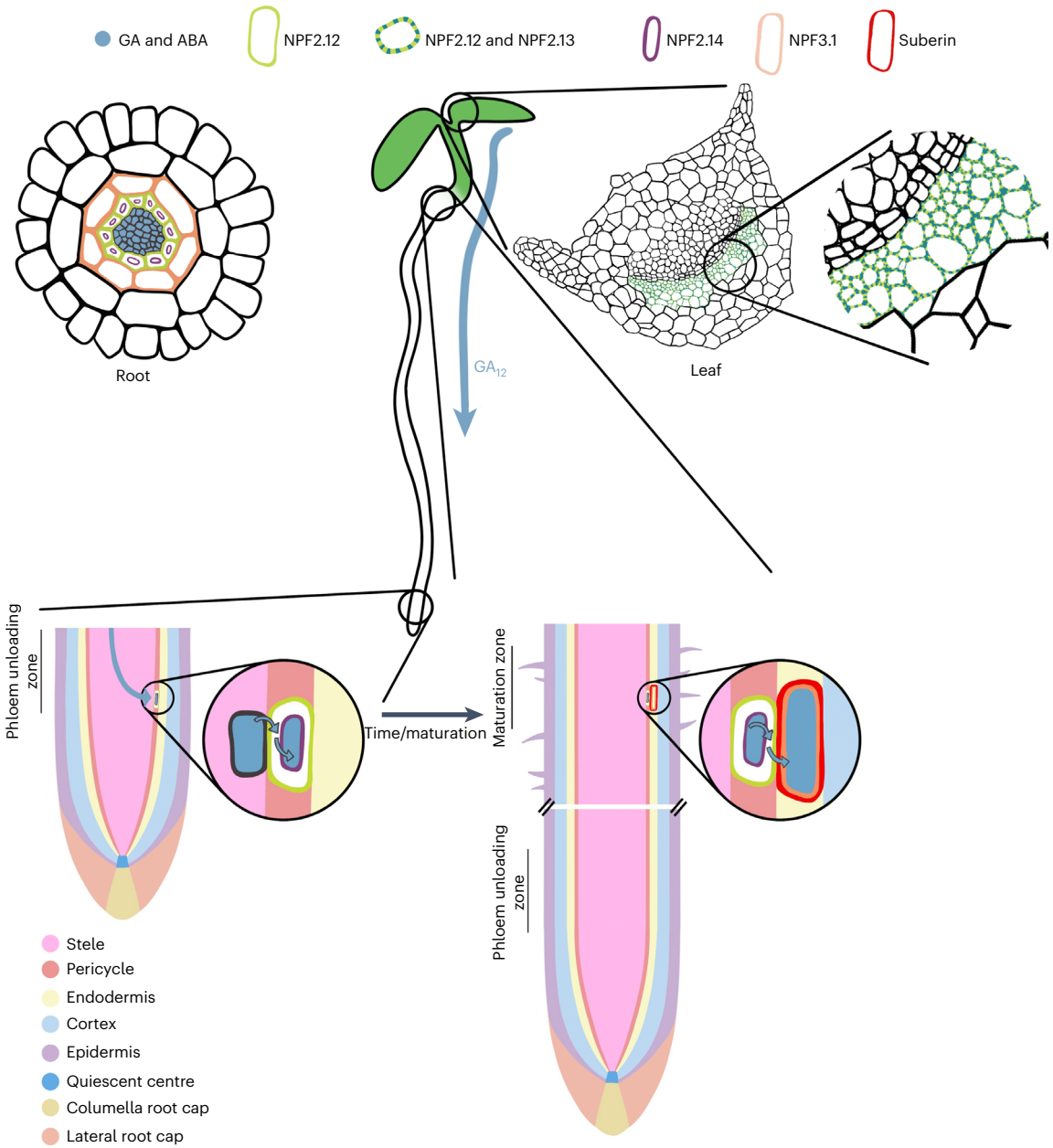

Fig. 7 | Proposed model illustrating that NPF2.12, NPF2.13, NPF2.14 and NPF3.1 function in regulating endodermal suberin formation. Proposed model incorporating experimentally observed distributions of root GA transporters, hormone accumulation, endodermal suberin formation and mathematical model predictions. NPF2.12 and NPF2.13, which are localized to the shoot phloem, are both required for GA_{12} long-distance shoot-to-root translocation. NPF2.12 is expressed in the root pericycle cell membranes and promotes the movement of ABA and GA from the vasculature to the pericycle. Once in the pericycle cytoplasm, NPF2.14 imports the hormones into the vacuole to form a reservoir that will be available at later stages. When the root elongates over time and the cells that accumulated high levels of GA and ABA in the vacuoles mature, the hormones are exported out of the pericycle vacuole and imported into the endodermis by NPF3.1 to induce suberization.

best of our knowledge, NPF2.14 is presumably the first known subcellular GA/ABA transporter. We showed that *NPF2.14* is expressed in the pericycle to facilitate endodermal root suberization. Oocyte experiments showing that NPF2.14 exports GA from the cytosol, combined with NPF2.14's localization to the tonoplast, indicate that NPF2.14 transports GA and ABA from the cytosol into the vacuole.

The results presented here suggest that the pericycle serves as a buffer zone, regulating the transitions of hormones from the stele to the endodermis (Fig. 7). The stele acts as the source of bioactive GA and ABA in the root[55,59]. Both hormones have been shown to accumulate and affect their respective responses specifically in the endodermis[25,28,60,61]. In addition, it appears that the GA and ABA do not simply flow through the pericycle but rather are loaded into the vacuole by NPF2.14 to form a reservoir for later developmental stages. We propose that the high levels of GA and ABA present in the phloem unloading zone are taken into the pericycle by NPF2.12. Once in the pericycle cells, NPF2.14 facilitates their import into the vacuole for storage. We speculate that a slow-release mechanism feeds the differentiating cells with GA and ABA, thus allowing suberin formation in the mature root (Fig. 7). Vacuoles have been proposed to act as storage, modification or degradation compartments for plant hormones[62]. It is possible that tonoplast-localized NPF2.14 mediates the hormonal homeostasis

balance that is needed for the proper execution of the developmental plan in the neighbouring cell file. At this point, it is not clear whether GA and ABA are stored in their bioactive form in the vacuole.

Confocal imaging of the NLS-YFP lines indicated that both *NPF2.12* and *NPF2.14* are expressed in the pericycle, mainly at the phloem poles (Figs. 2a and 4a). It is therefore possible that the hormone uptake is not carried out uniformly throughout the pericycle ring, but rather amplified at the pericycle phloem pole cells. If so, do the two hormones retain polar distribution in the pericycle and in the subsequent endodermis layer? Or do the hormones have the ability to move within the two cell file rings? Future mathematical models and genetic work is required to address these questions.

The significantly reduced GA_{12} content in *npf2.12 npf2.13* double knockout phloem extracts implies that these transporters are required for GA_{12} loading into the phloem and translocation of GA_{12} from the shoot to the root. Thus, we hypothesize that NPF2.12 and NPF2.13, which are plasma membrane-localized importers expressed in the shoot phloem companion cells, are part of the long-sought mediators of long-distance GA shoot-to root translocation. Our results agree with the previous finding that GA_{12} is the main form of GA that is transported long distances through the plant[12]. In addition, we showed that GA3ox1 and GA3ox2, which catalyse the final step of active GA production, are expressed in the root stele[55] (Fig. 5f). Thus, once GA_{12} docks at the root stele, it is converted by GA3ox1 and GA3ox2 into the bioactive GA_4 form, which is then delivered from the stele to the endodermis by NPF2.12 and NPF3.1 (Fig. 6c).

It is intriguing that NPF2.12 and NPF2.13 act as GA_{12} shoot-to-root transporters and also promote the delivery of the bioactive forms of GA and ABA to the endodermis. In both cases, a plasma membrane import activity is involved, but the substrate specificity differs. Since we showed that NPF2.12 and NPF2.13 can transport both intermediates of and the bioactive forms of GA (Fig. 3b, and Supplementary Figs. 9 and 10) and that GA_{12} is present at high levels in the shoot phloem (Fig. 5a), we speculate that GA_{12} is the primary substrate of the transporters. In the root stele, NPF2.12 recognizes bioactive ABA and GA_4, which are present in high concentrations due to being synthesized there[59].

The presented work show apparently for the first time that GA deficiency results in lower endodermal suberization and can be complemented by GA or ABA. This result is interesting at multiple points of view. First, it may explain the physiological importance of GA accumulation in the endodermis. Second, it suggests that GA and ABA function non-antagonistically to promote endodermis suberization. At this stage, it is not clear whether GA promotes endodermis suberization directly by, for example, direct binding and activation of suberin biosynthesis factors by DELLA or DELLA co-partners, or whether suberization is a secondary effect of maturation or signalling through the ABA components. Our result in oocytes suggesting that GA enhances ABA import may point to another possibility where there is co-activity in regulating suberin formation at the transport level of the two hormones. While GA and ABA are considered antagonistic hormones[63], it is possible that that the two hormones can act non-antagonistically to promote root suberization by dual-transport activity of the hormones. How GA promotes ABA import biochemically from the transport structure/function point of view is not clear at the moment. The non-antagonistic results between the two hormones agree with the growth defects displayed by biosynthesis mutants of these hormones, which result in small dark green plants[64–66]. Thus, it could be that in a specific context where GA and ABA transport plays a role, the two hormones act synergistically.

Methods

Plant material and growth conditions

All *Arabidopsis thaliana* lines are in a Col-0 background. T-DNA insertion lines were supplied by the *Arabidopsis* Biological Resource Center. PCR genotyping for homozygous lines was performed using the primers listed in Supplementary Table 1. To generate the *npf2.12 npf2.13* double mutant, *npf2.12* (SALK_138987) was crossed with *npf2.13* (SALK_022429) to obtain an F_1 population. F_3 homozygous plants were selected by PCR genotyping. Additional T-DNA lines described in this study: *npf2.12* (SALK_104042c) and *npf2.13*: (SALK_053264). To generate the triple *npf2.12 npf2.13 npf2.14* mutant, a CRISPR/Cas9 construct targeting *NPF2.14* was introduced into the *npf2.12 npf2.13* double-mutant background.

Plants were sown on vertical plates containing 0.5× Murashige-Skoog (MS) medium, 1% sucrose and 0.8% agar (pH 5.7), stratified for 2 d at 4 °C in the dark, then transferred to growth chambers (Percival CU41L5) at 21 °C and 100 µE m^{-2} s^{-1} light intensity under long day light (16 h light/8 h dark). All plants in suberin quantification experiments were grown on 0.5× MS medium, 1% sucrose and 0.8% agar (pH 5.7) for 3 d and subsequently moved to 0.5× MS medium without sucrose supplementation due to phenotype masking by the sucrose treatment. For low-nitrate experiments, plants were sown on nitrate-free MS with vitamins (Caisson labs MSP07-50LT), which was supplemented with 0.01 mM (low nitrate) or 10 mM (high nitrate) KNO_3.

CRISPR

To generate the CRISPR/Cas9 vector targeting *NPF2.14*, the MoClo system was implemented. Cloning of the *NPF2.14*-specific guide (guide sequence: ATTGTTGTCTCGTCGTTAAATCCG) into the system was done according to ref. 67.

Hypocotyl cross-sections

Sectioning and clearing were performed as previously described[44]. Hypocotyls (3-week-old) were fixed in 4% PFA for an hour, rinsed twice in 1× PBS embedded in 5% agarose and sectioned to 150 µM slices using a Leica VT1000S vibratome. Slices were cleared using a ClearSee solution for 5 d. Following clearing, sections were counterstained with 0.1% calcofluor white in ClearSee solution for 30 min. Next, the seedlings were washed in ClearSee for 30 min with gentle shaking. For imaging, sections were mounted directly in ClearSee and imaged using a Zeiss LSM 780 inverted microscope.

Hormone application

Hormone was added to the agar medium at concentrations indicated in the figure legends. Seedlings were either germinated on media or moved after germination to treatment plates. GA-Fl (5 µM) was applied in liquid MS media for 16 h before imaging. For *ga1* experiments, both Col-0 and *ga1* seeds were imbibed in sterile water containing 5 µM GA_3 for 16 h to induce uniform germination. Following imbibition, seeds were washed three times in sterile water to wash away excess GA and sown on MS plates.

Cloning of NPFs overexpression and reporter lines

NPF2.12 and *NPF2.14* coding sequences were synthesized by Bio Basic, cloned into pENTR/D-TOPO (Invitrogen K2400) and subsequently cloned into the pH7YWG2 destination vectors using the LR Gateway reaction (Invitrogen 11791). *NPF2.12* and *NPF2.14* promoters were amplified with the primers listed in Supplementary Table 2 using a Phusion high-fidelity polymerase (New England Biolabs), cloned into pENTR/D-TOPO, and then cloned into pMDC7 vector for *NLS-YFP* reporters and pGWB3 vector for GUS reporters.

To generate *pNPF2.13:GUS* reporter, the promoter of *NPF2.13* (1.7-kb fragment) was PCR amplified from Col-0 genomic DNA with appropriate primers listed in Supplementary Table 2, inserted into pDONR221 (Invitrogen) by Gateway cloning and recombined with pGWB633[68].

Imaging and analysis

Seedlings were stained in 10 mg l^{-1} propidium iodide (PI) for 5 min, rinsed and mounted in water. Seedlings were imaged using a laser

scanning confocal microscope (Zeiss LSM 780 inverted microscope), with argon laser set at 488 nm for fluorescein, 514 nm for YFP and 561 nm for PI excitation. Emission filters used were 493–548 nm for fluorescein derivatives, 508–570 nm for YFP and 583–718 nm for PI emission. Image analysis and signal quantification were done with the measurement function of ZEN lite software. The number of quantified biological repeats and sampling points is indicated for each graph in figure legends. All statistical analyses and graphs were made using GraphPad Prism v8.

Root length characterization

For root length measurements, seedlings were imaged using a Zeiss Stemi 2000-C stereo microscope and measured using ImageJ software (http://rsbweb.nih.gov/ij/index.html).

Histochemical GUS staining

Plants were immersed in 100 mM sodium phosphate buffer (pH 7.0) containing 0.1% Triton X-100, 1 mM 5-bromo-4-chloro-3-indolyl-β-D-glucuronic acid cyclohexylammonium salt (Sigma Aldrich), 2 mM potassium ferricyanide and 2 mM potassium ferrocyanide. Plants were subjected to vacuum treatment for 10 min and then incubated at 37 °C for 16 h. Tissues were cleared with 30%, 50% and 70% ethanol for 30 min in each concentration and imaged using an AxioZoom 16 Zeiss binocular microscope.

For cross-sectioning of GUS-stained leaf petioles, after clearing in 70% ethanol, the samples were fixed in FAA solution (3.2% formaldehyde, 5% acetic acid, 50% ethanol) for 30 min and kept overnight at 4 °C. The samples were then dehydrated in an ethanol gradient ranging from 50% to 96% and incubated in 2% eosin overnight at 4 °C. After several washes in 96% ethanol, the samples were progressively rehydrated in ethanol/HISTO-CLEAR II (Electron Microscopy Sciences) solution, incubated in 50% HISTO-CLEAR II 50% PARAPLAST PLUS (McCormick Scientific) at 60 °C for 2 h and embedded in 100% PARAPLAST PLUS. Paraffin-embedded samples were cross-sectioned with a LEICA RM2155 microtome and imaged using a Leica Leitz Dmrb microscope.

Nile red suberin staining, imaging and quantification

Nile red suberin staining was performed as previously described[44]. Briefly, 5-day-old seedlings were fixed in paraformaldehyde for 1 h under gentle agitation and washed twice in phosphate-buffered saline at pH 7.4. Plants were covered in filtered 0.05% Nile red (Acros Organics, 7385-67-3) solution dissolved in ClearSee for 16 h. Following staining, plants were washed three times in ClearSee for 30 min per wash. Next, plants were counterstained with 0.1% calcofluor white (Glentham Life Sciences, 4404-43-7) dissolved in ClearSee for cell wall imaging. After 30 min, plants were washed in ClearSee for 30 min. Plants were mounted directly in ClearSee on slides and imaged with a Zeiss LSM 780 confocal microscope. Images were taken from the upper part of the root and under the root-hypocotyl junction with an argon laser set at 514 nm for Nile red excitation and 405 nm for calcofluor excitation. Emission filters used were 561–753 nm filter for Nile red and 410–511 nm filter for calcofluor emission. Fluorescence intensity was assessed from 5 endodermal cells per root using the Zen software.

For root patterning, following Nile red staining, roots were imaged using an AxioZoom 16 Zeiss binocular microscope. Root length and length of continuously and patchily suberized zones were measured using ImageJ. Percent of suberized area was normalized to total root length. All statistical analyses and graphs were made using GraphPad Prism v8.

RT–qPCR

Total RNA was isolated from the indicated plant materials using RNeasy Plant mini kit (QIAGN 74,904). DNA was removed by RQ1 RNase-free DNase (Promega M6101). Total RNA (2 µg) was converted to complementary DNA (cDNA) using M-MLV Reverse Transcriptase (Promega M1701) with oligo(dT)15 primer according to manufacturer protocols. RT–qPCR was performed with 40 ng cDNA in a final volume of 10 µl with Fast SYBR Green Master Mix (ABI 4385612) using the Step One Plus system and software (ABI). The reaction conditions included 40 amplification cycles (3 s at 95 °C, 30 s at 60 °C). Three technical repeats were performed for each cDNA sample, and at least three biological repeats were used for each treatment. Relative quantification was calculated using the ΔΔCt method, with PP2A used as the reference gene. Primers are specified in Supplementary Table 3.

Phylogenetic tree

Protein sequences for *Arabidopsis thaliana* NPF family members were retrieved from TAIR (https://www.arabidopsis.org). Phylogenetic relationships were defined using Phylogeny.fr (http://www.phylogeny.fr/) and visualized with FigTree software (http://tree.bio.ed.ac.uk/software/figtree/).

Transport assays in *Xenopus* oocytes

Coding sequences were cloned into the pNB1u vector, and complementary RNA (cRNA) was produced as previously described[34]. *Xenopus* oocyte assays were performed as previously described[34]. Defolliculated *X. laevis* oocytes (stage V–VI) were purchased from Ecocyte Biosciences, injected with 25 ng cRNA in 50.6 nl using a Drummond Nanoject II and incubated for 2–4 d at 16 °C in HEPES-based kulori (90 mM NaCl, 1 mM KCl, 1 mM $MgCl_2$, 1 mM $CaCl_2$, 5 mM HEPES (pH 7.4)) before use. Oocytes were pre-incubated in MES-based kulori (90 mM NaCl, 1 mM KCl, 1 mM $MgCl_2$, 1 mM $CaCl_2$, 5 mM MES (pH 5)) for 4 min and then transferred to phytohormone-containing MES-based kulori for 60 min. After washing three times in 25 ml HEPES-based kulori followed by one wash in 25 ml deionized water, oocytes were homogenized in 50% methanol and stored for >30 min at −20 °C. Following centrifugation (25,000 *x g* for 10 min 4 °C), the supernatant was mixed with deionized water to a final methanol concentration of 20% and filtered through a 0.22 µm filter (MSGVN2250, Merck Millipore) before analytical LC–MS/MS as described below. For nitrate assays, sodium chloride in kulori was substituted for equimolar sodium nitrate so as not to affect the membrane potential.

Quantification of phytohormone content by LC–MS/MS

Compounds in the diluted oocyte extracts were directly analysed by LC–MS/MS. The analysis was performed following a previously described method[16] with modifications. In brief, chromatography was performed on an Advance UHPLC system (Bruker). Separation was achieved on a Phenomenex Kinetex 1.7u XB-C18 column (100 × 2.1 mm, 1.7 µm, 100 Å) with 0.05% (v/v) formic acid in water as mobile phase A and acetonitrile with 0.05% formic acid (v/v) as mobile phase B. The gradients used for elution of GAs were 0–0.5 min, 2% B; 0.5–1.3 min, 2–30% B; 1.3–2.2 min 30–100% B, 2.2–2.8 min 100% B; 2.8–2.9 min 100-2% B; and 2.9–4.0 min 2% B. The gradients used for elution of ABA were 0–0.5 min, 2% B; 0.5–1.2 min, 2–30% B; 1.2–2.0 min, 30–100% B; 2.0–2.5 min, 100% B; 2.5–2.6 min, 100-2% B; and 2.6–4.0 min, 2% B. The mobile phase flow rate was 400 µl min^{-1} and column temperature was maintained at 40 °C. The liquid chromatography was coupled to an EVOQ Elite triple quadrupole mass spectrometer (Bruker) equipped with an electrospray ion source operated in positive and negative ionization mode. Instrument parameters were optimized by infusion experiments with pure standards. For analysis of GAs, the ion spray voltage was maintained at +4,000 V and −4,000 V in positive and negative ionization mode, respectively, and the heated probe temperature was set to 200 °C with probe gas flow at 50 psi. For ABA, the ion spray voltage was maintained at −3,300 V in negative ionization mode, and heated probe temperature was set to 120 °C with probe gas flow at 40 psi. Remaining settings were identical for all analytical methods with cone temperature set to 350 °C and cone gas to 20 psi. Nebulizing gas was set to 60 psi and collision gas to 1.6 mTorr. Nitrogen was

used as probe and nebulizing gas, and argon as collision gas. Active exhaust was constantly on. Multiple reaction monitoring was used to monitor analyte parent ion to product ion transitions for all analytes. Multiple reaction monitoring transitions and collision energies were optimized by direct infusion experiments. Detailed values for mass transitions can be found in Supplementary Table 4. Both Q1 and Q3 quadrupoles were maintained at unit resolution. Bruker MS Workstation software (v8.2.1) was used for data acquisition and processing. Linearity in ionization efficiencies was verified by analysing dilution series of standard mixtures. Sinigrin glucosinolate was used as internal standard for normalization but not for quantification. Quantification of all compounds was achieved using external standard curves diluted with the same matrix as the actual samples. All GAs were analysed together in a single method. GA_{12} suffered from severe ion suppression when combined with the other GAs in the standard curve, thus quantification was not achieved for GA_{12}.

Root suberin monomer profiling by GC–MS

Suberin monomers were extracted from Col-0 and mutant roots according to previously described protocols[69,70]. A sample volume of 1 µl was injected in splitless mode on a GC–MS system (Agilent 7693A Liquid Auto injector, 8860 gas chromatograph and 5977B mass spectrometer). GC was performed (HP-5MS UI column; 30 m length, 0.250 mm diameter and 0.25 µm film thickness; Agilent J&W GC columns) with injection temperature of 270 °C, interface set to 250 °C and the ion source to 200 °C. Helium was used as the carrier gas at a constant flow rate of 1.2 ml min^{-1}. The temperature programme was 0.5 min isothermal at 70 °C, followed by a 30 °C min^{-1} oven temperature ramp to 210 °C and a 5 °C min^{-1} ramp to 330 °C, then kept constant during 21 min. Mass spectra were recorded with an *m/z* of 40 to 850 scanning range. Chromatograms and mass spectra were evaluated using the MSD ChemStation software (Agilent). Integrated peaks of mass fragments were normalized for sample dry weight and the respective C32 alkane internal standard signal. For identification, the corresponding mass spectra and retention time indices were compared with the NIST20 library as well as in-house spectral libraries.

Xenopus oocyte injection-based efflux transport assays and competition assays

For injection-based export assays, on the second day of gene expression, oocytes were injected with 23 nl 8.2 mM in 98 mM KCl, 1 mM $CaCl_2$ and 10 mM HEPES (pH 7.4). T1 oocytes were left to heal for 10 min and then transport was evaluated as described above. T2 oocytes were left for approximately 20 h in HEPES-based kulori at 16 °C, followed by transport analysis.

Quantification of nitrate from oocytes by HPLC

Nitrate concentration in the oocyte extracts was quantified using a Dionex ICS-2100 anion exchange chromatography system (Thermo Fisher). The separation was done on a Dionex IonPac AG11-HC analytical column coupled to the AS11-HC guard column (Thermo Fisher). The columns were connected to a Dionex AERS 500 anion suppressor (Thermo Fisher). The analyses were performed under the following conditions: sample injection volume of 4.8 µl, column temperature of 30 °C, flow rate of 0.38 ml min^{-1}, isocratic eluent gradient using 30 mM KOH solution in QH_2O, suppressor current of 29 mA and runtime of 15 min. Nitrate detection was done at 220 nm using a Dionex UltiMate 3000 (Thermo Fisher). QH_2O water dilutions of Dionex Combined Seven Anion Standard (Thermo Fisher) were used to create a standard calibration curve. Accuracy and precision of the quantification was checked by including samples of potassium nitrate throughout the sequence.

pH measurements of oocyte lumen

Stabilization of pH was performed as described previously[34]. pH electrodes were pulled from borosilicate glass capillaries (KWIK-FIL TW F120–3 with filament) on a vertical puller (Narishige), baked for 120 min at 220 °C and silanized for 60 min with dimethyldichlorosilane (Silanization Solution I, Sigma Aldrich). Electrodes were backfilled with a buffer containing 40 mM KH_2PO_4, 23 mM NaOH and 150 mM NaCl (pH 7.5). The electrode tip was filled with a proton-selective ionophore cocktail (hydrogen ionophore I cocktail A, Sigma Aldrich) by dipping the tip into the cocktail. Oocytes, as described above, were placed in freshly made HEPES-based ekulori (2 mM $LaCl_3$, 90 mM NaCl, 1 mM KCl, 1 mM $MgCl_2$, 1 mM $CaCl_2$, 5 mM HEPES (pH 7.4)) for at least 30 min before three-electrode voltage clamp experiments. Before each oocyte measurement, a pH calibration curve was made for each oocyte using 100 mM KCl pH 5.5, 100 mM KCl pH 6.5 and 100 mM KCl pH 7.5. Oocytes were clamped at 0 mV and perfused with HEPES-based ekulori pH 7.4, followed by MES-based ekulori (2 mM $LaCl_3$, 90 mM NaCl, 1 mM KCl, 1 mM $MgCl_2$, 1 mM $CaCl_2$, 5 mM MES (pH 5)) and internal pH response was measured continuously as a function of external pH change.

Membrane potential measurements

Membrane potentials of oocytes were measured in ekulori (90 mM NaCl, 1 mM KCl, 1 mM $MgCl_2$, 1 mM $CaCl_2$, 5 mM MES, 2 mM $LaCl_3$ (pH 5)) using the automated two-electrode voltage clamp system, Roboocyte2 (Multi Channel Systems), with electrodes backfilled with 1 M KCl and 1.5 M potassium acetate. All oocytes were measured using the same electrodes with a resistance of 280–350 kΩ. The experiment was terminated when the resistance of one of the electrodes shifted to approximately 600 kΩ.

Two-electrode voltage clamp electrophysiology

The electric signal elicited by GA treatment of oocytes was measured in ekulori (90 mM NaCl, 1 mM KCl, 1 mM $MgCl_2$, 1 mM $CaCl_2$, 5 mM MES, 2 mM LaCl3 (pH 4.5 or pH 5)) using Roboocyte2 (Multi Channel Systems), with electrodes (resistance 280–1,000 kΩ) backfilled with 1 M KCl and 1.5 M potassium acetate. Oocytes were clamped at −60 mV, and IV (Current-Voltage) curves were obtained before and after substrate addition. Substrate dependent currents were calculated by subtracting currents before addition of substrate from currents after addition of substrate.

Root hormone quantification

Hormone extraction and analysis was performed as previously described[33]. Standards (both labelled and non-labelled) were obtained from Olchemim and the National Research Council (NRC-CNRC, Canada). Standard-grade solvents methanol, acetic acid (LiChrosolv, Sigma Aldrich), acetonitrile (J.T.Baker), formic acid (Honeywell Fluka, Thermo Fisher) and deionized water (Milli-Q, Synergy-UV millipore system) were used for sample preparation. Briefly, root tissue frozen in liquid nitrogen was grounded using a mortar and pestle. Around 200 mg of root sample was measured from ground powder and extracted with ice-cold methanol:water:formic acid (15:4:1 v/v/v) added with deuterium-labelled internal standards. Similar concentrations of internal standards of abscisic acid and gibberellin (GA_4) were added into samples and calibration standards. The samples were purified using Oasis MCX SPE cartridges (Waters) according to manufacturer protocol. The samples were injected on an Acquity UPLC BEH C18 column (1.7 µm, 2.1 × 100 mm (Waters); with gradients of 0.1% acetic acid in water or acetonitrile) connected to an Acquity UPLC H class system (with Waters Acquity QSM, FNR sample manager and PDA) coupled with a UPLC–ESI–MS/MS triple quadrupole mass spectrometer (Xevo TQ-S (Waters), equipped with an ESI probe) for identification and quantification of hormones. The hormones were measured using an MS detector, both in positive and negative mode, with two MRM (Multiple Reaction Monitoring) transitions for each compound. External calibration curves were constructed with hormone standards added with internal standards, used for quantification and calculated using Target Lynx (v4.1; Waters) software by

comparing the ratios of MRM peak areas of the analyte to those of the internal standard.

Phloem extract and hormone quantification

Rosette leaves of 5-week-old Col-0 and *npf2-12 npf2-13* mutant plants (before bolting) were cut with a razor blade at the base of the petiole, and each leaf was dipped in a tube containing 80 µl of exudation buffer (50 mM potassium phosphate buffer (pH 7.6), 10 mM EDTA). Exudation was carried out for 3 h in the dark at high humidity to limit transpiration. Exudation of 75 leaves was regrouped and concentrated under vacuum centrifugation. Hormone contents of phloem exudates were determined using UPLC–MS/MS (Waters Quattro Premier XE). Concentrated residue of phloem sap was resuspended in 80% methanol-1% acetic acid including 17-$^{2}H_{2}$-labelled GA internal standards (Olchemim), mixed and passed through an Oasis HLB column. The dried eluate was dissolved in 5% acetonitrile-1% acetic acid, and the GAs were separated by UHPLC chromatography (Accucore RP-MS column 2.6 µm, 100 × 2.1 mm; Thermo Fisher) with a 5 to 50% acetonitrile gradient containing 0.05% acetic acid, at 400 µl min^{-1} over 22 min. The concentrations of GAs in the extracts were analysed with a Q-Exactive mass spectrometer (Orbitrap detector; Thermo Fisher) by targeted SIM (Selected Ion Monitoring) using embedded calibration curves and the Xcalibur 2.2 SP1 build 48 and TraceFinder programmes.

Grafting assays

Grafting was performed without collars on water imbibed 0.45 µM MCE membrane (Millipore) between hypocotyls of rootstocks and scions of 6-day-old seedlings grown on 1× MS agar plate. Grafted seedlings were then kept vertically to recover for 5 d under constant humidity. Successful grafts were transferred onto ½× MS agar plates and grown under a 16 h photoperiod at 22 °C. Root growth was measured every day for 3 d with ImageJ (https://imagej.nih.gov/ij/download.html). Nile red suberin staining fluorescence intensity was assessed as previously described, in roots of 13-day-old grafted seedlings 2 d after transfer onto ½× MS agar plates.

DELLA degradation assays

Seedlings (12-day-old) were transferred to 1× MS agar modified medium without nitrogen (bioWORLD plant media) supplemented with 0.5 mM KNO_3 and 1 µM paclobutrazol (Sigma). At 4 d after transfer, a drop of GA_{12} (5 µl at 1 µM) was placed on one of the first two leaves formed. Roots were collected at 6, 12 and 24 h after adding GA_{12}. Total proteins were extracted in 2× SDS–PAGE sample buffer and separated on 10% SDS–PAGE gel. After transfer onto membranes, immunoblots were performed using a 2,000-fold dilution of anti-RGA (Agrisera) and a 10,000-fold dilution of peroxidase-conjugated goat anti-rabbit (Thermo Fisher). Signals were detected with Fusion FX (Vilber) using Immobilon Forte Western HRP Substrate (Millipore). The blot was subsequently stained with Coomassie blue. Quantification of the signals was performed using ImageJ.

Mathematical model

Root templates were segmented from an experimental image using the CellSeT image analysis tool[71] (Supplementary Fig. 21). We used CellSeT to manually assign a cell type to each cell and then read the geometrical and cell-type data into a tissue database (based on the OpenAlea tissue structure[72]), extending the data structure to incorporate vacuolar compartments within each cell. The geometrical, topological and transporter-distribution data were used to form a system of ordinary differential equations to describe the GA transport, synthesis and degradation within the multicellular root cross-section. Parameters associated with the passive and transporter-mediated transport components were estimated using the oocyte data (Figs. 1a and 3b) and the remaining parameter values were obtained from the literature (Supplementary Table 5). These ordinary differential equations were simulated using the solve_ivp package in Python 3.6.5. Full details of the model equations and assumptions are provided as Supplementary text.

Reporting summary

Further information on research design is available in the Nature Portfolio Reporting Summary linked to this article.

Data availability

All the data supporting the findings of this study are available within the Article and its Supplementary Information. Source data are provided with this paper. The python code used to produce the model results is available at: https://gitlab.com/leahband/ga_aba_transport_rootcrosssection_model.

References

1. Hedden, P. & Sponsel, V. A century of gibberellin research. *J. Plant Growth Regul.* **34**, 740–760 (2015).
2. Eriksson, S., Böhlenius, H., Moritz, T. & Nilsson, O. GA4 is the active gibberellin in the regulation of LEAFY transcription and *Arabidopsis* floral initiation. *Plant Cell* **18**, 2172–2181 (2006).
3. Proebsting, W. M., Hedden, P., Lewis, M. J., Croker, S. J. & Proebsting, L. N. Gibberellin concentration and transport in genetic lines of pea: effects of grafting. *Plant Physiol.* **100**, 1354–1360 (1992).
4. Björklund, S., Antti, H., Uddestrand, I., Moritz, T. & Sundberg, B. Cross-talk between gibberellin and auxin in development of *Populus* wood: gibberellin stimulates polar auxin transport and has a common transcriptome with auxin. *Plant J.* **52**, 499–511 (2007).
5. Dayan, J. et al. Leaf-induced gibberellin signaling is essential for internode elongation, cambial activity, and fiber differentiation in tobacco stems. *Plant Cell* **24**, 66–79 (2012).
6. Chin, T. Y. & Lockhart, J. A. Translocation of applied gibberellin in bean seedlings. *Am. J. Bot.* **52**, 828–833 (1965).
7. Zweig, G., Yamaguchi, S. & Mason, G. W. in *GIBBERELLINS. Advances in Chemistry* Vol. 28 122–134 (American Chemical Society, 1961).
8. Hoad, G. V. & Bowen, M. R. Evidence for gibberellin-like substances in phloem exudate of higher plants. *Planta* **82**, 22–32 (1968).
9. Hu, J. et al. Potential sites of bioactive gibberellin production during reproductive growth in *Arabidopsis*. *Plant Cell* **20**, 320–336 (2008).
10. Weiss, D. & Halevy, A. H. Stamens and gibberellin in the regulation of corolla pigmentation and growth in *Petunia hybrida*. *Planta* **179**, 89–96 (1989).
11. Hedden, P. & Thomas, S. G. Gibberellin biosynthesis and its regulation. *Biochem. J.* **444**, 11–25 (2012).
12. Regnault, T. et al. The gibberellin precursor GA12 acts as a long-distance growth signal in *Arabidopsis*. *Nat. Plants* **1**, 1–6 (2015).
13. Camut, L. et al. Root-derived GA12 contributes to temperature-induced shoot growth in *Arabidopsis*. *Nat. Plants* **5**, 1216–1221 (2019).
14. Chiba, Y. et al. Identification of *Arabidopsis thaliana* NRT1/PTR FAMILY (NPF) proteins capable of transporting plant hormones. *J. Plant Res.* **128**, 679–686 (2015).
15. Kanno, Y. et al. AtSWEET13 and AtSWEET14 regulate gibberellin-mediated physiological processes. *Nat. Commun.* **7**, 1–11 (2016).
16. Tal, I. et al. The *Arabidopsis* NPF3 protein is a GA transporter. *Nat. Commun.* **7**, 1–11 (2016).
17. Saito, H. et al. The jasmonate-responsive GTR1 transporter is required for gibberellin-mediated stamen development in *Arabidopsis*. *Nat. Commun.* **6**, 1–11 (2015).

18. Corratgé-Faillie, C. & Lacombe, B. Substrate (un)specificity of *Arabidopsis* NRT1/PTR FAMILY (NPF) proteins. *J. Exp. Bot.* **68**, 3107–3113 (2017).
19. Nour-Eldin, H. H. et al. NRT/PTR transporters are essential for translocation of glucosinolate defence compounds to seeds. *Nature* **488**, 531–534 (2012).
20. Kramer, E. M. How far can a molecule of weak acid travel in the apoplast or xylem? *Plant Physiol.* **141**, 1233–1236 (2006).
21. Binenbaum, J., Weinstain, R. & Shani, E. Gibberellin localization and transport in plants. *Trends Plant Sci.* **23**, 410–421 (2018).
22. Zhu, J. K. Abiotic stress signaling and responses in plants. *Cell* **167**, 313–324 (2016).
23. Cutler, S. R., Rodriguez, P. L., Finkelstein, R. R. & Abrams, S. R. Abscisic acid: emergence of a core signaling network. *Annu. Rev. Plant Biol.* **61**, 651–679 (2010).
24. Liu, X. & Hou, X. Antagonistic regulation of ABA and GA in metabolism and signaling pathways. *Front. Plant Sci.* **9**, 251 (2018).
25. Ubeda-Tomás, S. et al. Root growth in *Arabidopsis* requires gibberellin/DELLA signalling in the endodermis. *Nat. Cell Biol.* **10**, 625–628 (2008).
26. Ubeda-Tomás, S. et al. Gibberellin signaling in the endodermis controls *Arabidopsis* root meristem size. *Curr. Biol.* **19**, 1194–1199 (2009).
27. Duan, L. et al. Endodermal ABA signaling promotes lateral root quiescence during salt stress in *Arabidopsis* seedlings. *Plant Cell* **25**, 324–341 (2013).
28. Shani, E. et al. Gibberellins accumulate in the elongating endodermal cells of *Arabidopsis* root. *Proc. Natl Acad. Sci. USA* **110**, 4834–4839 (2013).
29. David, L. C. et al. N availability modulates the role of NPF3.1, a gibberellin transporter, in GA-mediated phenotypes in *Arabidopsis*. *Planta* **244**, 1315–1328 (2016).
30. Andersen, T. G., Barberon, M. & Geldner, N. Suberization — the second life of an endodermal cell. *Curr. Opin. Plant Biol.* **28**, 9–15 (2015).
31. Shukla, V. & Barberon, M. Building and breaking of a barrier: suberin plasticity and function in the endodermis. *Curr. Opin. Plant Biol.* **64**, 102153 (2021).
32. Barberon, M. The endodermis as a checkpoint for nutrients. *New Phytol.* **213**, 1604–1610 (2017).
33. Zhang, Y. et al. ABA homeostasis and long-distance translocation are redundantly regulated by ABCG ABA importers. *Sci. Adv.* **7**, eabf6069 (2021).
34. Wulff, N. et al. An optimized screen reduces the number of GA transporters and provides insights into Nitrate Transporter 1/Peptide Transporter family substrate determinants. *Front. Plant Sci.* **0**, 1106 (2019).
35. Jørgensen, M. E. et al. A functional EXXEK motif is essential for proton coupling and active glucosinolate transport by NPF2.11. *Plant Cell Physiol.* **56**, 2340–2350 (2015).
36. Solcan, N. et al. Alternating access mechanism in the POT family of oligopeptide transporters. *EMBO J.* **31**, 3411–3421 (2012).
37. Tsay, Y. F., Schroeder, J. I., Feldmann, K. A. & Crawford, N. M. The herbicide sensitivity gene CHL1 of *Arabidopsis* encodes a nitrate-inducible nitrate transporter. *Cell* **72**, 705–713 (1993).
38. Campilho, A., Nieminen, K. & Ragni, L. The development of the periderm: the final frontier between a plant and its environment. *Curr. Opin. Plant Biol.* **53**, 10–14 (2020).
39. Beeckman, T., Burssens, S. & Inze, D. The peri-cell-cycle in *Arabidopsis*. *J. Exp. Bot.* **52**, 403–411 (2001).
40. Takano, J. et al. *Arabidopsis* boron transporter for xylem loading. *Nature* **420**, 337–340 (2002).
41. Ross-Elliott, T. J. et al. Phloem unloading in *Arabidopsis* roots is convective and regulated by the phloempole pericycle. *eLife* **6**, e24125 (2017).
42. Wunderling, A. et al. A molecular framework to study periderm formation in *Arabidopsis*. *New Phytol.* **219**, 216–229 (2018).
43. Barberon, M. et al. Adaptation of root function by nutrient-induced plasticity of endodermal differentiation. *Cell* **164**, 447–459 (2016).
44. Ursache, R., Andersen, T. G., Marhavý, P. & Geldner, N. A protocol for combining fluorescent proteins with histological stains for diverse cell wall components. *Plant J.* **93**, 399–412 (2018).
45. Lux, A., Morita, S., Abe, J. & Ito, K. An improved method for clearing and staining free-hand sections and whole-mount samples. *Ann. Bot.* **96**, 989–996 (2005).
46. Kreszies, T., Schreiber, L. & Ranathunge, K. Suberized transport barriers in *Arabidopsis*, barley and rice roots: from the model plant to crop species. *J. Plant Physiol.* **227**, 75–83 (2018).
47. Woolfson, K. N., Esfandiari, M. & Bernards, M. A. Suberin biosynthesis, assembly, and regulation. *Plants* **11**, 555 (2022).
48. Aloni, R. Vascular Differentiation and Plant Hormones (Springer, 2021).
49. Wang, C. et al. Developmental programs interact with abscisic acid to coordinate root suberization in *Arabidopsis*. *Plant J.* **104**, 241–251 (2020).
50. Sunai', T.-P. & Kamiya, Y. The *Arabidopsis* GA1 locus encodes the cyclase ent-kaurene synthetase A of gibberellin biosynthesis. *Plant Cell* **6**, 1509–1518 (1994).
51. Lin, Q. et al. The SnRK2-APC/CTE regulatory module mediates the antagonistic action of gibberellic acid and abscisic acid pathways. *Nat. Commun.* **6**, 1–10 (2015).
52. Almagro, A., Lin, S. H. & Tsay, Y. F. Characterization of the *Arabidopsis* Nitrate Transporter NRT1.6 reveals a role of nitrate in early embryo development. *Plant Cell* **20**, 3289–3299 (2009).
53. Fan, S. C., Lin, C. S., Hsu, P. K., Lin, S. H. & Tsay, Y. F. The *Arabidopsis* Nitrate Transporter NRT1.7, expressed in phloem, is responsible for source-to-sink remobilization of nitrate. *Plant Cell* **21**, 2750–2761 (2009).
54. Sun, T. P. The molecular mechanism and evolution of the GA–GID1–DELLA signaling module in plants. *Curr. Biol.* **21**, R338–R345 (2011).
55. Barker, R. et al. Mapping sites of gibberellin biosynthesis in the *Arabidopsis* root tip. *New Phytol.* **229**, 1521–1534 (2021).
56. Band, L. R. et al. Systems analysis of auxin transport in the *Arabidopsis* root apex. *Plant Cell* **26**, 862–875 (2014).
57. Mathieu, Y. et al. Regulation of vacuolar pH of plant cells I. Isolation and properties of vacuoles suitable for 31P NMR studies. *Plant Physiol.* **89**, 19–26 (1989).
58. Hedrich, R., Mueller, T. D., Becker, D. & Marten, I. Structure and function of TPC1 vacuole SV channel gains shape. *Mol. Plant* **11**, 764–775 (2018).
59. Kuromori, T., Sugimoto, E. & Shinozaki, K. Intertissue signal transfer of abscisic acid from vascular cells to guard cells. *Plant Physiol.* **164**, 1587–1592 (2014).
60. De Diego, N. et al. Immunolocalization of IAA and ABA in roots and needles of radiata pine (*Pinus radiata*) during drought and rewatering. *Tree Physiol.* **33**, 537–549 (2013).
61. Ondzighi-Assoume, C. A., Chakraborty, S. & Harris, J. M. Environmental nitrate stimulates abscisic acid accumulation in *Arabidopsis* root tips by releasing it from inactive stores. *Plant Cell* **28**, 729–745 (2016).
62. Martinoia, E., Meyer, S., De Angeli, A. & Nagy, R. Vacuolar transporters in their physiological context. *Annu Rev. Plant Biol.* **63**, 183–213 (2012).
63. Shu, K., Zhou, W., Chen, F., Luo, X. & Yang, W. Abscisic acid and gibberellins antagonistically mediate plant development and abiotic stress responses. *Front. Plant Sci.* **9**, 416 (2018).

64. Peng, J. & Harberd, N. P. Gibberellin deficiency and response mutations suppress the stem elongation phenotype of phytochrome-deficient mutants of Arabidopsis. *Plant Physiol.* **113**, 1051–1058 (1997).
65. González-Guzmán, M. et al. The short-chain alcohol dehydrogenase ABA2 catalyzes the conversion of xanthoxin to abscisic aldehyde. *Plant Cell* **14**, 1833–1846 (2002).
66. Merilo, E. et al. Stomatal VPD response: there is more to the story than ABA. *Plant Physiol.* **176**, 851–864 (2018).
67. Engler, C. et al. A golden gate modular cloning toolbox for plants. *ACS Synth. Biol.* https://doi.org/10.1021/sb4001504 (2014).
68. Nakamura, S. et al. Gateway binary vectors with the bialaphos resistance gene, bar, as a selection marker for plant transformation. *Biosci. Biotechnol. Biochem.* **74**, 1315–1319 (2014).
69. Cohen, H. et al. A multilevel study of melon fruit reticulation provides insight into skin ligno-suberization hallmarks. *Plant Physiol.* **179**, 1486–1501 (2019).
70. Cohen, H., Fedyuk, V., Wang, C., Wu, S. & Aharoni, A. SUBERMAN regulates developmental suberization of the *Arabidopsis* root endodermis. *Plant J.* **102**, 431–447 (2020).
71. Pound, M. P., French, A. P., Wells, D. M., Bennett, M. J. & Pridmorea, T. P. CellSeT: novel software to extract and analyze structured networks of plant cells from confocal images. *Plant Cell* **24**, 1353 (2012).
72. Pradal, C. et al. OpenAlea: a visual programming and component-based software platform for plant modelling. *Funct. Plant Biol.* **35**, 751–760 (2008).

Acknowledgements

We thank D. Binenbaum for the illustrations and P. Hedden (Rothamsted Research) for sharing *pGA3ox1-4:GUS* seeds. This work was supported by grants from the Israel Science Foundation (2378/19 and 3419/20 to E.S.), the Human Frontier Science Program (HFSP—RGY0075/2015 and HFSP—LIY000540/2020 to E.S., H.H.N.-E. and L.R.B.), Danmarks Grundforskningsfond (DNRF99 to H.H.N.-E.), the European Research Council (757683-RobustHormoneTrans to E.S.), the Constantiner Travel Fellowship (to J.B.), the Centre National de la Recherche Scientifique (to L.S-A. J-M.D. and P.A.) and the French Ministry of Research and Higher Education studentship (to L.C.).

Author contributions

J.B. performed the research and wrote the manuscript. N.W. performed the oocyte transporter assays. L.C., L.S-A., J-M.D. and P.A. carried out long-distance transport assays. K.K. performed the mathematical modelling. I.T. assisted in cloning overexpression and reporter lines. H.V. and A.A. quantified root GA and ABA content. M.A. helped with genotyping T-DNA mutant lines and profiling suberin patterning. Y.Z. helped with *npf* mutant identification. D.R. and L.R. assisted in cross-sectioning and staining. E.C. quantified hormone content in the phloem sap. E.M. and H.C. performed suberin monomer quantifications. S.L. and R.W. synthesized fluorescently tagged hormones. S.B.Y. carried out the qPCR and created hormone-treated reporter lines. V.N. and C.C. helped with nitrate and hormone quantification in oocyte assays, respectively. C.H. carried out hormone competition transport assays. L.R.B., P.A., H.H.N.-E. and ES designed and supervised the work and edited the manuscript. All authors discussed the results and commented on the manuscript.

Competing interests

The authors declare no competing interests.

Additional information

Supplementary information The online version contains supplementary material available at https://doi.org/10.1038/s41477-023-01391-3.

Correspondence and requests for materials should be addressed to Leah R. Band, Patrick Achard, Hussam Hassan Nour-Eldin or Eilon Shani.

Peer review information *Nature Plants* thanks Benoît Lacombe, Marie Barberon and Eiji Nambara for their contribution to the peer review of this work.

nature portfolio

Corresponding author(s): Shani

Last updated by author(s): Mar 7, 2023

Reporting Summary

Nature Portfolio wishes to improve the reproducibility of the work that we publish. This form provides structure for consistency and transparency in reporting. For further information on Nature Portfolio policies, see our Editorial Policies and the Editorial Policy Checklist.

Statistics

For all statistical analyses, confirm that the following items are present in the figure legend, table legend, main text, or Methods section.

n/a	Confirmed	
☐	☒	The exact sample size (*n*) for each experimental group/condition, given as a discrete number and unit of measurement
☐	☒	A statement on whether measurements were taken from distinct samples or whether the same sample was measured repeatedly
☐	☒	The statistical test(s) used AND whether they are one- or two-sided *Only common tests should be described solely by name; describe more complex techniques in the Methods section.*
☐	☒	A description of all covariates tested
☐	☒	A description of any assumptions or corrections, such as tests of normality and adjustment for multiple comparisons
☐	☒	A full description of the statistical parameters including central tendency (e.g. means) or other basic estimates (e.g. regression coefficient) AND variation (e.g. standard deviation) or associated estimates of uncertainty (e.g. confidence intervals)
☐	☒	For null hypothesis testing, the test statistic (e.g. *F*, *t*, *r*) with confidence intervals, effect sizes, degrees of freedom and *P* value noted *Give P values as exact values whenever suitable.*
☐	☒	For Bayesian analysis, information on the choice of priors and Markov chain Monte Carlo settings
☒	☐	For hierarchical and complex designs, identification of the appropriate level for tests and full reporting of outcomes
☒	☐	Estimates of effect sizes (e.g. Cohen's *d*, Pearson's *r*), indicating how they were calculated

Our web collection on statistics for biologists contains articles on many of the points above.

Software and code

Policy information about availability of computer code

Data collection	Microscopy: ZEN Imaging Software (Zeiss LSM780); PLAZA 3.0 (http://bioinformatics.psb.ugent.be/plaza/)
Data analysis	Statistical analysis: GraphPad Prism v.8 Florescence intensity: ImageJ 1.53e Mathematical nodel: Simulation used the solve_ivp package in python 3.6.5

For manuscripts utilizing custom algorithms or software that are central to the research but not yet described in published literature, software must be made available to editors and reviewers. We strongly encourage code deposition in a community repository (e.g. GitHub). See the Nature Portfolio guidelines for submitting code & software for further information.

Data

Policy information about availability of data

All manuscripts must include a data availability statement. This statement should provide the following information, where applicable:

- Accession codes, unique identifiers, or web links for publicly available datasets
- A description of any restrictions on data availability
- For clinical datasets or third party data, please ensure that the statement adheres to our policy

All the data supporting the findings of this study are available within the article and its Supplementary Information files.

Human research participants

Policy information about studies involving human research participants and Sex and Gender in Research.

Reporting on sex and gender	Not relevant
Population characteristics	Not relevant
Recruitment	Not relevant
Ethics oversight	Not relevant

Note that full information on the approval of the study protocol must also be provided in the manuscript.

Field-specific reporting

Please select the one below that is the best fit for your research. If you are not sure, read the appropriate sections before making your selection.

☒ Life sciences ☐ Behavioural & social sciences ☐ Ecological, evolutionary & environmental sciences

For a reference copy of the document with all sections, see nature.com/documents/nr-reporting-summary-flat.pdf

Life sciences study design

All studies must disclose on these points even when the disclosure is negative.

Sample size	Sample size is described for each experiment. In general, we tried to apply the highest N number possible, depending on the experiment feasibility.
Data exclusions	Data was not excluded
Replication	All findings were successfully reproduced in several replicates. The number of replication for each experiment is indicated in Source data file. All imaging assays were performed at least 3 times with similar results, as indicated in the legends of each Figure.
Randomization	All genotypes and treatments were randomized (position in plates). Multiple replications of genotypes and treatments were carried across each experiment.
Blinding	Due to the nature of the experimental setup and automated code analysis, blinding was not applicable

Reporting for specific materials, systems and methods

We require information from authors about some types of materials, experimental systems and methods used in many studies. Here, indicate whether each material, system or method listed is relevant to your study. If you are not sure if a list item applies to your research, read the appropriate section before selecting a response.

Materials & experimental systems

n/a	Involved in the study
☐	☒ Antibodies
☒	☐ Eukaryotic cell lines
☒	☐ Palaeontology and archaeology
☒	☐ Animals and other organisms
☒	☐ Clinical data
☒	☐ Dual use research of concern

Methods

n/a	Involved in the study
☒	☐ ChIP-seq
☒	☐ Flow cytometry
☒	☐ MRI-based neuroimaging

Antibodies

Antibodies used	anti-RGA (Agrisera) and a 10000-fold dilution of peroxidase-conjugated goat anti-rabbit (Thermo Fisher Scientific)
Validation	The antibodies were previously reported and validated, Regnault, Thomas, et al. "The gibberellin precursor GA12 acts as a long-distance growth signal in Arabidopsis." Nature Plants 1.6 (2015): 1-6.